iScience

CellPress
OPEN ACCESS

Article

Experimental evidence and clinical implications of Warburg effect in the skeletal muscle of Fabry disease

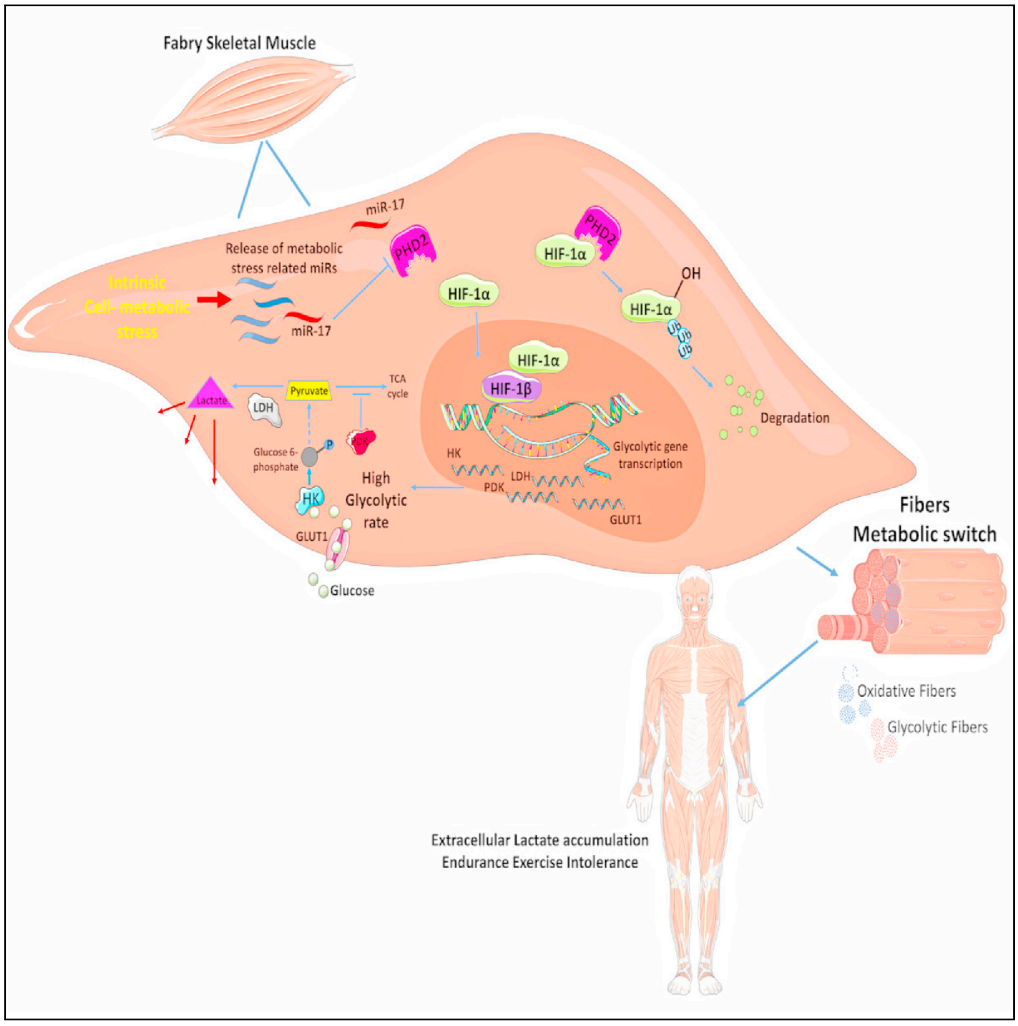

Jessica Gambardella, Antonella Fiordelisi, Federica Andrea Cerasuolo, ..., Gaetano Santulli, Daniela Sorriento, Guido Iaccarino

guiaccar@unina.it

Highlights

FD mice and patients show intolerance to aerobic activity and lactate accumulation

A metabolic remodeling occurs in FD muscle with a glycolytic switch

miR-17 mediated HIF-1 upregulation is responsible for the Warburg effect in FD muscle

Exercise testing, blood lactate, and miR-17 are useful for monitoring FD

Gambardella et al., iScience 26, 106074
March 17, 2023
https://doi.org/10.1016/j.isci.2023.106074

iScience

CellPress
OPEN ACCESS

Article

Experimental evidence and clinical implications of Warburg effect in the skeletal muscle of Fabry disease

Jessica Gambardella,[1,2] Antonella Fiordelisi,[1] Federica Andrea Cerasuolo,[1] Antonietta Buonaiuto,[1] Roberta Avvisato,[1] Alessandro Viti,[1] Eduardo Sommella,[3] Fabrizio Merciai,[3] Emanuela Salviati,[3] Pietro Campiglia,[3] Valeria D'Argenio,[4,5] Silvia Parisi,[6] Antonio Bianco,[2] Letizia Spinelli,[2] Eugenio Di Vaia,[1] Alberto Cuocolo,[1] Antonio Pisani,[7] Eleonora Riccio,[7] Teodolinda Di Risi,[7] Michele Ciccarelli,[8] Gaetano Santulli,[9,10] Daniela Sorriento,[1,2] and Guido Iaccarino[1,2,11,*]

SUMMARY

Skeletal muscle (SM) pain and fatigue are common in Fabry disease (FD). Here, we undertook the investigation of the energetic mechanisms related to FD-SM phenotype. A reduced tolerance to aerobic activity and lactate accumulation occurred in FD-mice and patients. Accordingly, in murine FD-SM we detected an increase in fast/glycolytic fibers, mirrored by glycolysis upregulation. In FD-patients, we confirmed a high glycolytic rate and the underutilization of lipids as fuel. In the quest for a tentative mechanism, we found HIF-1 upregulated in FD-mice and patients. This finding goes with miR-17 upregulation that is responsible for metabolic remodeling and HIF-1 accumulation. Accordingly, miR-17 antagomir inhibited HIF-1 accumulation, reverting the metabolic-remodeling in FD-cells. Our findings unveil a Warburg effect in FD, an anaerobic-glycolytic switch under normoxia induced by miR-17-mediated HIF-1 upregulation. Exercise-intolerance, blood-lactate increase, and the underlying miR-17/HIF-1 pathway may become useful therapeutic targets and diagnostic/monitoring tools in FD.

INTRODUCTION

Fabry disease (FD, OMIM 301500) is a rare lysosomal storage disorder caused by pathogenic variants in the *GLA* gene encoding the constitutive enzyme α-galactosidase A (α-Gal A).[1] Deficient or absent α-Gal A enzyme and the subsequent lysosomal accumulation of glycosphingolipids, primarily globotriaosylceramides, cause progressive organ damage with life-threatening complications and increased risk of premature death.[2–6] FD is a systemic disease with a wide spectrum of heterogeneously progressive clinical phenotypes; this spectrum ranges from the "classic" severe phenotype in males to a seemingly asymptomatic disease observed in females, with a variety of clinical presentations in between.[7–12] Pain is one of the earliest clinical symptoms of FD, also reported by children and young adults,[13,14] and life-impacting pain may still be present despite long-term enzyme replacement therapy (ERT), thereby requiring the use of adjunctive medications. Exercise intolerance even to mild physical activity has been reported in FD patients,[7,15,16] occurring also in the absence of a marked left ventricle hypertrophy, making this sign independent of cardiac impairment, such as diastolic dysfunction.[9] Rather, exercise intolerance might indicate the direct involvement of skeletal muscle. Indeed, alterations of skeletal myocytes have been reported in young and minimally symptomatic FD subjects.[9,17,18] Albeit muscular symptoms represent one of the main presenting features of FD, preceding the onset of cardiomyopathy and chronic kidney dysfunction,[19] the skeletal muscle in FD has been hitherto poorly investigated.[20,21] This unmet research need should be considered, given the likely high impact of skeletal muscle alterations on FD patients' quality of life, as recently acknowledged.[22,23] Few single-case reports describe muscular abnormalities in FD patients but do not elucidate the pathogenesis and the underlying molecular mechanisms.[17,18,24] Energetic alterations could be involved, because the metabolic capability of the skeletal muscle is a key determinant of muscular performance, and alterations of energetic metabolism have been observed in cells from FD patients.[25] Similarly, several genetic myopathies, characterized by exercise intolerance and fatigue, are associated with disruptions of metabolic flexibility of skeletal muscle.[24–26] Specifically, a switch in muscular fiber

[1]Department of Advanced Biomedical Sciences, Federico II University, Naples, Italy

[2]Interdepartmental Center of Research on Hypertension and Related Conditions (*CIRIAPA*), Federico II University, Naples, Italy

[3]Department of Pharmacy, University of Salerno, Salerno, Italy

[4]Department of Human Sciences and Quality of Life Promotion, San Raffaele Open University, Rome, Italy

[5]CEINGE- Advanced Biotechnologies, Naples, Italy

[6]Department of Molecular Medicine and Medical Biotechnologies, Federico II University, Naples, Italy

[7]Department of Public Health, Federico II University, Naples, Italy

[8]Department of Medicine and Surgery, University of Salerno, Salerno, Italy

[9]Department of Medicine, Division of Cardiology, Wilf Family Cardiovascular Research Institute, Einstein Institute for Aging Research, Albert Einstein College of Medicine, New York, NY, USA

[10]Department of Molecular Pharmacology, Fleischer Institute for Diabetes and Metabolism (*FIDAM*), Einstein-Mount Sinai Diabetes Research Center (*ES-DRC*), Einstein Institute for Neuroimmunology and Inflammation, Albert Einstein College of Medicine, New York, NY, USA

[11]Lead contact

*Correspondence: guiaccar@unina.it

https://doi.org/10.1016/j.isci.2023.106074

subtype together with a marked reliance on anaerobic metabolism with lactate over-production are described in genetic myopathies.[26] Despite the primary alterations of FD skeletal muscle and several pieces of evidence indicating metabolic stress,[25,27,28] the chance to consider FD a genetic myopathy has never been explored.

The transcription factor hypoxia-inducible factor-1 (HIF-1) is a key regulator of metabolic capability of skeletal muscle, promoting anaerobic metabolism in physiological and pathological conditions, including several genetic myopathies.[29] Canonically, HIF-1 supports muscle adaptation to hypoxia by stimulating the expression of glycolytic transporters and enzymes, thus warranting a high glycolytic rate.[30,31] Indeed, in presence of oxygen, proline-hydroxylases (PDH 1–3) are activated, triggering the ubiquitination and degradation of the HIF-1α subunit, thereby inhibiting HIF-1.[32] However, several alternative routes allow HIF-1 activation in presence of oxygen, a phenomenon known as Warburg Effect.[33–38] Many non-hypoxic stimuli are capable of turning on HIF-1, including hormones, growth factors, and microRNAs (miRs), and usually mediate HIF-1α stabilization by targeting PDH2. For instance, Chen et al. observed that miR-17 directly downregulate PDH2, therefore increasing HIF-1α levels.[39] In this scenario, HIF-1 acts as the metabolic stress sensor driving cell metabolic remodeling in response to a plethora of conditions.

In FD, the presence of a metabolic stress is suggested by the upregulation of miR-17.[27,40] Hence, it is possible to speculate that the genetic defect in FD induces per se an intrinsic metabolic stress determining an abnormal remodeling of skeletal muscle metabolism with reduced performance and fatigability.

The present study aims to characterize the muscle phenotype associated with FD, including muscle metabolic capability and its impact on physical performance. We employed a humanized-mouse model of FD to directly assess muscle composition and metabolic profile. Then, we translated our findings in FD patients and in cells obtained from FD patients. Lastly, we explored the involvement of HIF-1/miR-17 axis as molecular mechanism in FD-associated metabolic remodeling, appraising the possibility to consider FD a new genetic myopathy.

RESULTS

Altered exercise tolerance and muscle fibers composition in FD mice

To evaluate the muscular phenotype in FD, we measured the physical performance of FD mice compared to age-matched control mice under both aerobic (endurance) and anaerobic (acute) workloads. We determined the propensity to aerobic activity by measuring the spontaneous overnight wheel-run; FD mice exhibited a marked reduction of the overnight run (Figure 1A) indicating a lower tolerance to aerobic activity compared to WT mice. To measure muscle output under acute workload, we performed a weight test, observing that FD-mice reached a higher score compared to control mice (Figure 1 B), demonstrating greater muscle power in sustaining acute/anaerobic exercise. In addition to this finding, under maximal effort we detected a larger accumulation of lactate in the blood of FD mice compared to WT, further suggesting the metabolic switch of FD skeletal muscle toward anaerobic glycolytic metabolism (Figure 1C).

By histological analyses, we directly determined the muscle fibers composition of FD-mice and controls. Fast/Type II anaerobic fibers were significantly more abundant in FD compared to WT-muscle tissue, at the expense of Type I/slow aerobic and intermediate fibers (Figures 1D and 1E). Therefore, the fiber composition of FD muscle mirrors the altered exercise tolerance and fatigability observed in FD.

Metabolic remodeling of FD skeletal muscle: High glycolytic rate and lactacid metabolism

We further explored the metabolic remodeling of skeletal muscle of FD mice by performing biochemical analyses on isolated muscle, to directly assess the switch toward anaerobic glycolysis. Compared to skeletal muscle from control mice, in FD we detected higher levels of Hexokinase II (HK, Figures 2A and 2B), the enzyme that catalyzes the first step of glycolysis; this finding is consistent with the biochemical events occurring in conditions of anaerobic metabolism (Warburg effect).[41] Pyruvate Dehydrogenase Kinase 1 (PDK1), which inhibits the entrance of pyruvate into the mitochondria and therefore favors lactacid metabolism, is significantly upregulated in FD muscle compared to WT (Figures 2A–2C). Additionally, lactate-dehydrogenase (LDH) which converts pyruvate into lactate, is upregulated in FD skeletal muscle (Figures 2A–2D);accordingly, we detected an accumulation of intramuscular lactate in FD mice (Figure 2E).

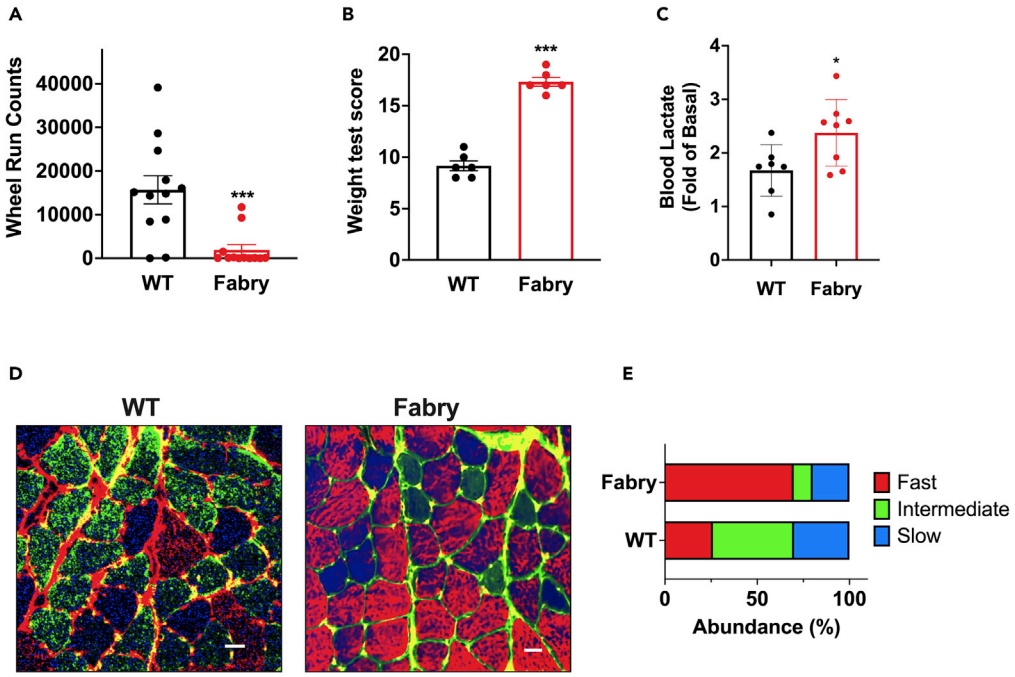

Figure 1. Spontaneous overnight wheel run was assessed in FD and control mice to measure physical activity propensity and endurance

Automatic count of mice wheel run (A). Muscle power and strength were assessed in FD and WT mice by performing a weight test. The score was proportional to the weight and time of handling (B). Blood lactate was detected at rest and after the maximal effort; the increment of lactate in response to exercise was reported as folds of basal (C). Immunofluorescence analysis on muscle sections from FD and WT mice was performed to determine fibers composition. A representative picture with red staining for fast fibers, blue staining for slow fibers, and green staining for intermediate fibers (Scale Bar: 50 μm) (D). Quantitative analysis of fibers composition expressed in percentage of abundance (E). Data are represented as mean ± SEM; *t* test: *p <0.05, ***p <0.0005.

The metabolic remodeling of skeletal muscle also affects the muscular capacity and selectivity in utilization of metabolites. Hence, we evaluated the pattern of glucose and fatty acid transporters in FD skeletal muscle. The insulin-dependent expression of Glucose transporter 4 (GLUT4) on cellular membranes was reduced, as shown by both immunofluorescence on intact tissue (Figure 3A) and immunoblot analysis of cellular membranes isolated from WT and FD skeletal muscles (Figures 3B and 3C). Conversely, insulin-independent GLUT1 membrane translocation was markedly increased in FD skeletal muscle (Figures 3A, 3B and 3C). The higher GLUT1/GLUT4 ratio demonstrates the increased constitutive capacity to uptake glucose of FD muscle, further suggesting its strict dependence on glucose. Accordingly, fasting glycemia was lower in FD mice compared to WT, reflecting the higher rate of glucose extraction (Figure S3A). In addition to these findings, levels of *p*-GSK3 (inactive form) were decreased in FD skeletal muscle, suggesting that also the insulin-induced glycogen synthesis is blocked and that the cell uses up as fuel all the uptaken glucose (Figure S3B).

Skeletal muscle uses fatty acids as an alternative to glucose for energy production. CD36 is the main muscular transporter of long-chain fatty acid (LCFA) into the cell,[42,43] and its expression was significantly reduced on membranes of FD myotubes compared to WT, as shown by immunofluorescence on muscular sections (Figure 3D).

Fatty acid synthase (FASN) is the key enzyme involved in the synthesis of palmitate from acetyl-CoA and malonyl-CoA,[44] and is downregulated in FD skeletal muscle compared with WT (Figure 3C). These findings indicate that the metabolism of FD skeletal muscle is less dependent on lipids, with a reduction of LCFA uptake and lipogenesis. Overall, the biochemical analysis confirmed the metabolic unbalance of FD skeletal muscle toward lactacid catabolism of glucose.

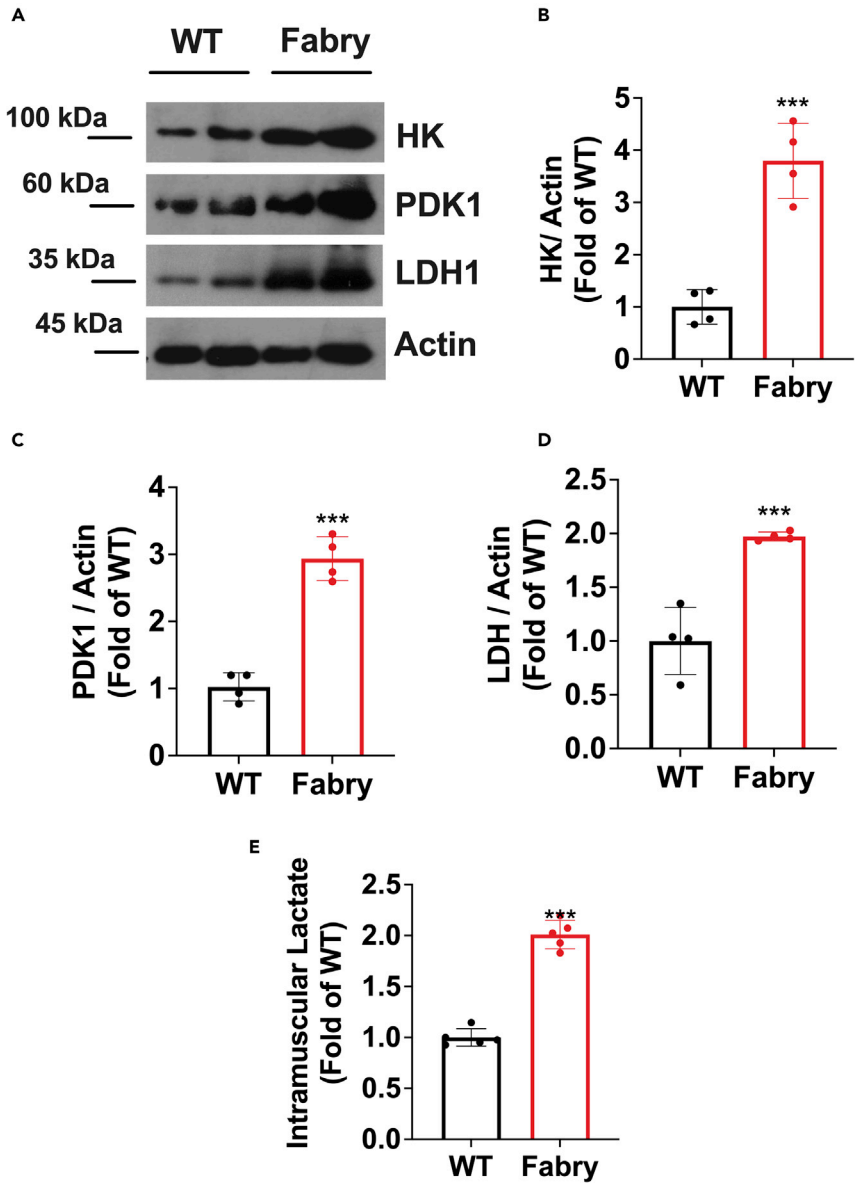

Figure 2. Western blot analysis on whole muscle lysate and detection of Hexokinase (HK), PDK1, and LDH1. Actin levels were used as the loading control

The pictures are representative of 3 independent experiments (A). Densitometric analysis of HK, PDK1, and LDH1 respective bands was performed. The ratio between the target and loading control (actin) was used as the normalized value to compare WT and FD mice (B–D). On whole muscle lysate, an immunoassay was conducted to evaluate the levels of intramuscular lactate. The total amount of proteins was used to normalize lactate levels (E). Data are represented as mean ± SEM; *t* test: ***p <0.0005.

Altered exercise tolerance and lactate accumulation in FD patients

To translate our findings to the clinical scenario, we assessed the tolerance of FD patients to physical stress to investigate muscle phenotype. We evaluated exercise intensity and duration in 58 FD patients compared to 30 age-matched controls. Specifically, we determined the duration of exercise achieved by the patients during a stress test on the cycle ergometer. The stress test was interrupted at 85% of theoretical heart rate or at muscle exhaustion, whichever occurred first. Clinical data of FD patients and healthy controls are depicted in Table 1. The mutations detected in our population of FD subjects are liste in Table 2. FD patients exhibited a shorter duration at the stress test compared to controls (Figure 4A). We measured capillary

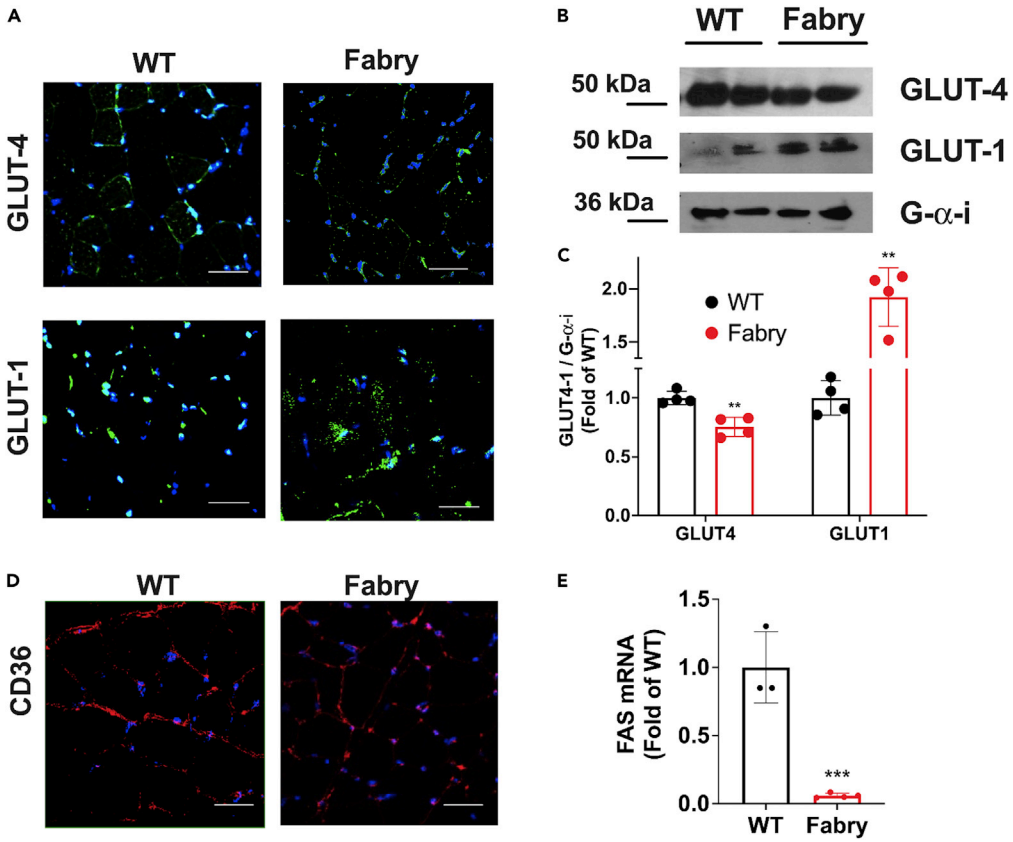

Figure 3. Immunofluorescent analysis on muscle sections from FD and WT mice was performed to determine the levels of glucose transporters (GLUT4/1)

Representative pictures with green staining for GLUT4 (up), GLUT1 (down), and blue for nuclear DAPI (A). Western blot analysis on membrane extracts from skeletal muscle and detection of GLUT4 and GLUT1. $G\alpha_i$ levels were used as loading control for membrane extract. The pictures are representative of 3 independent experiments (B). Densitometric analysis of GLUT4/1 respective bands was performed. The ratio between the target and loading control ($G\alpha_i$) was used as the normalized value to compare WT and FD mice (C). Immunofluorescence analyses on the muscular section of FD and WT mice were performed to determine the levels of fatty acid transporters CD36. A representative picture with red staining for CD36, and blue for nuclear DAPI (D) (scale bar: 50 μm). Real-time PCR was conducted on whole mRNAs isolated from FD and WT skeletal muscle. FASN mRNA was amplified and quantified from the total pool of mRNAs; 18s was used as a housekeeping gene to normalize the results (E). Data are represented as mean ± SEM; *t* test: **p <0.005, ***p <0.0005.

lactate before and at the exercise peak, and the increase in capillary lactate in response to the maximal exercise was higher in FD patients than in healthy controls (Figure 4B) (almost 4 times higher in FD). This finding strongly suggests that FD patients reached the maximal energetic expenditure by using glycolytic anaerobic metabolism and supports the idea that the muscular metabolic remodeling observed in FD mice occurs in human disease as well.

In a small pool of our FD population, we tested the effects of available FD therapies on exercise tolerance. Specifically, we retrospectively selected a subgroup of 11 patients who were followed for at least one year, and who were naive to FD treatment at enrollment. One subgroup of 5 patients started the treatment (age 56 ± 4 years, Body weight: 74 ± 7 kg; height: 168 ± 6 cm; female:3), whereas another subgroup of 6 patients (age 39 ± 6 years, body weight: 63 ± 4, height:165 ± 2 cm; female:6) did not start the treatment and the decision was procrastinated to the next follow-up based on anthropometric and clinical parameters and target organ involvement. The clinicians responsible for this decision were AP and ER. Patients were all evaluated at one-year follow-up. At baseline, the two subgroups of patients were already significantly different in terms of endurance, with reduced exercise duration recorded in the group who had started the therapy (Figure 4C). After one year, in not treated patients, exercise duration was comparable to the baseline, whereas in the treated subgroup we observed a significant improvement of exercise endurance

Table 1. Characteristics of FD and control populations

Characteristics	Controls	Patients
N	30	58
Age (years)	43 ± 19	42 ± 15
Gender (male, %)	71%	50%
Caucasian race (%)	100%	100%
Body weight (Kg)	74 ± 14	74± 17
Height (m)	1.71 ± 10	1.65 ± 16
FD treatment (Migalastat, Replagal, Fabrazyme)	N/A	57% (42%, 12%, 46%)

Data are expressed as mean ± SD or percent. Data were analyzed by t-test.
N/A, not applicable.

(Figure 4D). This finding confirms that the reduced tolerance to exercise is a specific and sensitive hallmark of FD, and that therapy can correct this feature, resulting particularly useful for monitoring the therapeutic response in FD patients.

Markers of anaerobic glycolytic metabolism are increased in FD patient-derived fibroblasts

One FD patient and his healthy first-degree relative underwent skin biopsies from which we isolated primary fibroblasts to be expanded *in vitro*. This approach allowed us to directly assess the biochemical signature of anaerobic glycolytic metabolism, in patient-derived cell lines, an approach never tested before. Of interest, human FD cells exhibited a higher expression of HK, PDK1, and LDH levels than control cells (Figures 4E and 4F), confirming the presence of the biochemical machinery able to support a high glycolytic rate. Accordingly, FD cells displayed higher membrane levels of GLUT-1 alongside with an increased glucose consumption rate then control cells (Figure S1A and S1B). Moreover, FD cells released more lactate, consistent with an increased extracellular acidification rate (ECAR) (Figures S1C and S1D). Taken together, these results strongly support a substantial hyperactivation of glycolysis in FD cells, eventually resulting in augmented lactate production; consistent with the data from FD skeletal muscle, this finding strengthens the idea that FD cells present a remodeling of the energetic metabolism supported preferentially by anaerobic glycolysis. This unique metabolic signature seems to be primitive and genetically determined, not dependent on cell type and environment.

Plasma metabolomic and lipidomic profile endorses the metabolic disarrangement in FD patients

To further validate the metabolic remodeling occurring in FD, we delineated the profile of metabolites and lipids in plasma from FD patients compared with controls, which is expected to mirror the muscular

Table 2. Panel of mutations identified in α-Gal A gene and their relative abundance in our FD population

Mutation	Effect on Protein translation	Functional consequences	% of patients
SNV c.901C>G	Nonsense mutation (p. Arg301*)	Effect on protein activity	40
SNV c.1066C>T	Missense mutation (p. Arg356Trp)	Effect on protein activity	31.6
SNV c.352C>T	Missense mutation (p.Arg118Cys)	Effect on protein activity	8.3
SNV c.950T>C	Missense mutation (p.Ile317Thr)	Uncertain	5
SNV c.508G>A	Missense mutation (p.Asp170Gly)	Effect on protein activity	5
SNV C.427G>A	Missense mutation (p.Ala143Thr)	Effect on protein activity	3.3
SNV c.680G>A	Missense mutation (p.Arg227Gln)	Effect on protein activity	1.7
SNV c.153G>A	Missense mutation (p.Met51Ile)	Uncertain	1.7
SNV c.667T>G	Missense mutation (p.Cys223Arg)	Uncertain	1.7
SNV c.388A>G	Missense mutation (p.Lys130Glu)	Uncertain	1.7

SNV, Single Nucleotide Variation; *, Premature stop codon and protein truncation; Uncertain, no functional evidence are available.

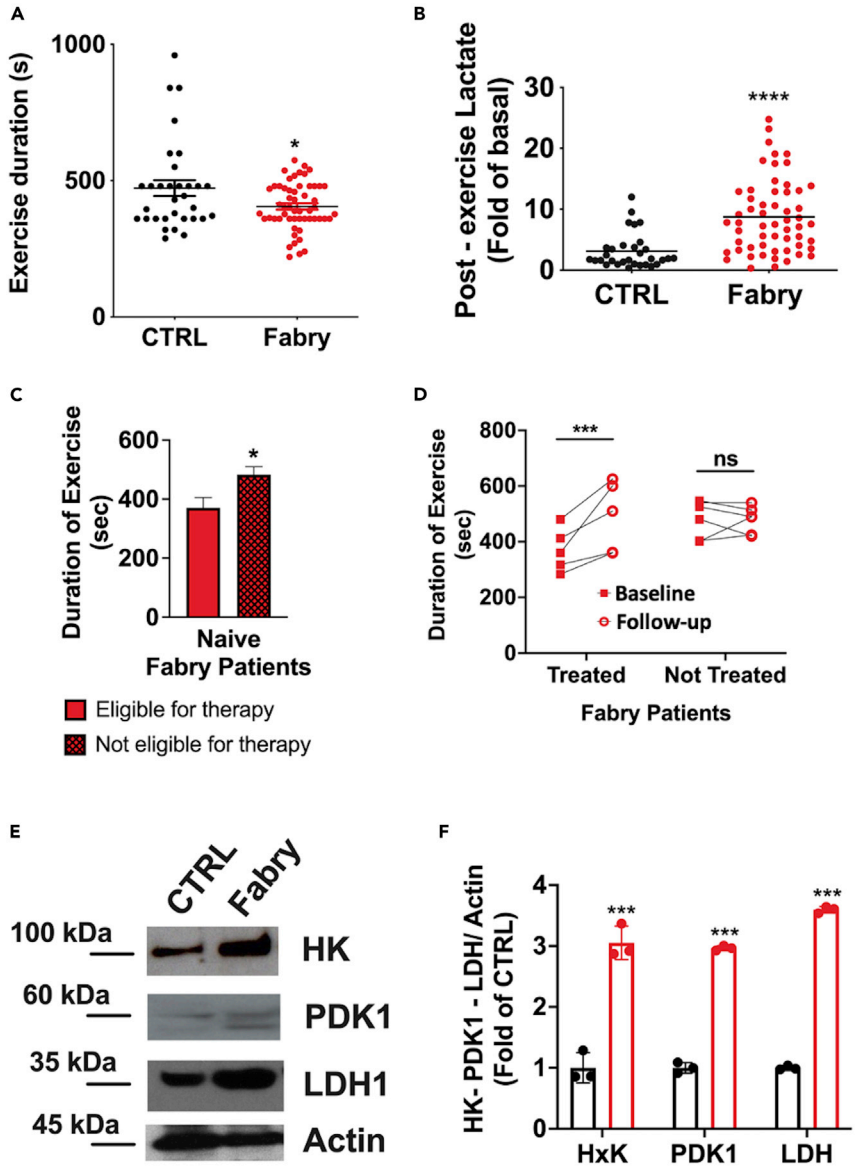

Figure 4. Exercise tolerance was assessed in FD patients and healthy controls by the Bruce test

The exercise intensity achieved by the patients was recorded and expressed as exercise duration (seconds) (A). Blood lactate was measured in Fabry and control subjects at rest, and after maximal effort. The accumulation of lactate in response to exercise was calculated as folds of baseline (post/pre) (B). Based on clinical manifestations, naive patients were stratified in eligible and not eligible for therapy and exercise duration was assessed in both subgroups. At baseline, patients with FD clinical phenotypes showed impaired exercise tolerance (C). The assessment of physical performance one year post-enrollment revealed a significant increase of exercise duration in patients of the treated group (D). Fibroblasts derived from skin biopsy were isolated from both an FD patient and a healthy relative (control). Western blot analysis was performed on whole cells lysate to detect the levels of Hexokinase (HK), PDK1 and LDH1. Actin levels were used as the loading control. The pictures are representative of 3 independent experiments (E). Densitometric analysis of HK, PDK1 and LDH1 respective bands was performed. The ratio between the target and loading control (actin) was used as the normalized value to compare WT and FD mice (F). Data are represented as mean ± SEM; *t* test: *p <0.05, ***p <0.0005, ****p <0.0001 Fabry vs CTRL (A-B-D-E), Eligible versus not eligible for therapy (C), After versus Before (D).

metabolic status.[45] High-resolution mass spectrometry was performed with an untargeted approach on both polar and non-polar plasma extract. FIA-FT-ICR-MS was carried out on polar fraction, and the resultant PLS-DA 2D-score plots showed a clear clustering of FD patients (Figure 5A). A heatmap reports the top

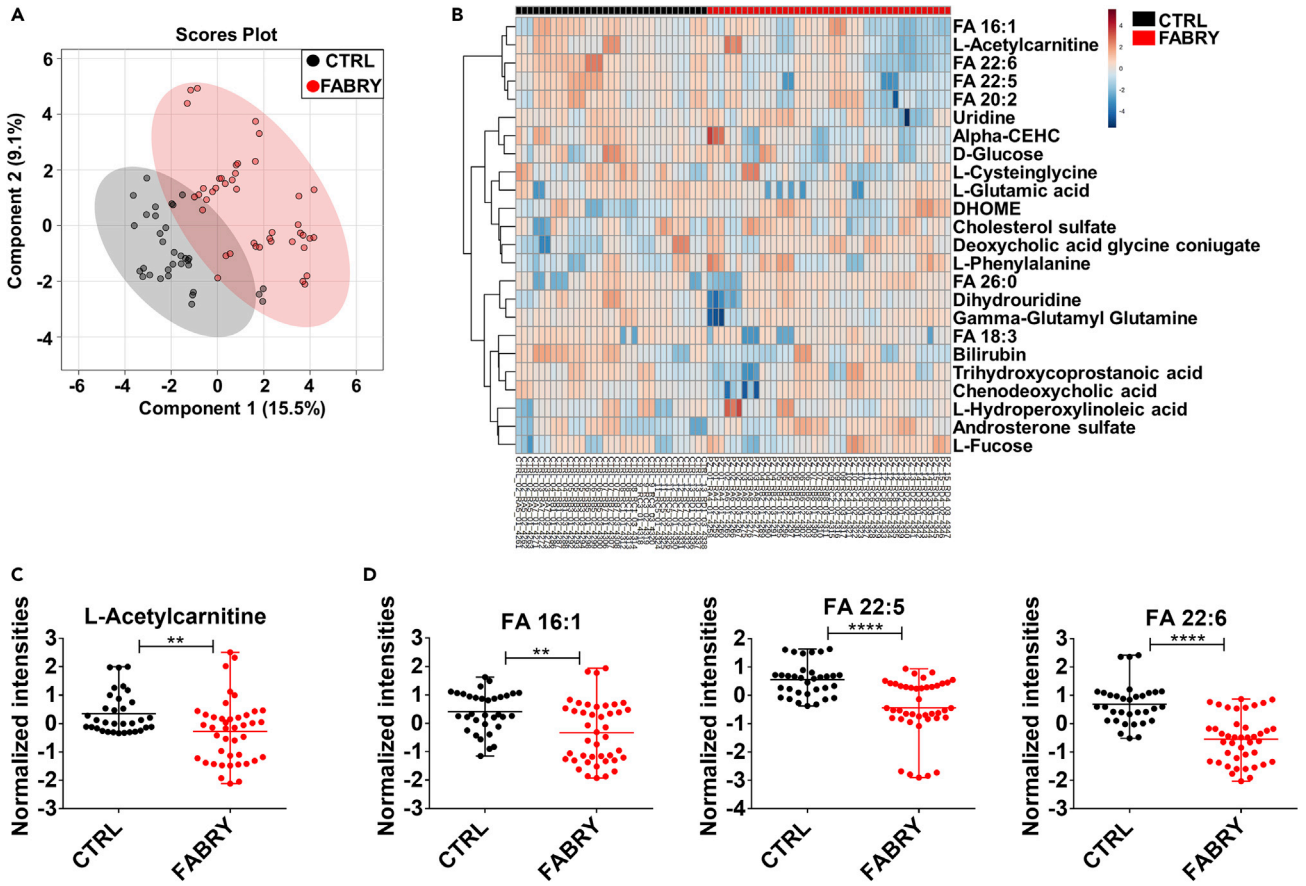

Figure 5. Metabolomic analysis was performed on plasma from FD and healthy controls by FT-ICR Mass spectrometry

Two-dimensional partial least-squares discriminant analysis (PLS-DA) score plots (A) of metabolome analysis determined using DI-HRMS showing clustering and separation between Controls (black) and FD (red) groups. (B) Heatmap of top statistically relevant metabolites ($p < 0.05$, FDR< 0.01), (C) normalized intensity of L-Acetylcarnitine; (D) normalized intesity of lipid substrates (FA: fatty acids) Data are represented as mean ± SD; *t* test: **p <0.005, ****p <0.0001.

24 metabolites showing significant differences in the relative abundance among the two groups (Figure 5B). Acetylcarnitines and fatty acids were the main affected classes with reduced levels in the FD population (Figures 5C and 5D), suggesting altered lipid metabolism.

The lipid fraction was analyzed by RP-UHPLC-TIMS-MS providing the lipidomic profile of plasma from FD patients compared with healthy controls. Again, FD patients generated an independent cluster (Figure 6A). Among the top 24 statistically significant features, several subclasses of lipids were dysregulated when comparing FD to controls, including triacyglycerols (TGs), phosphatidylcholines (PCs), sphingomyelins (SMs), and diacylglycerols (DGs) (Figure 6B). Specifically, we observed plasma accumulation of several TGs (Figure 6C), most likely attributable to their reduced tissue extraction and catabolism.[46,47] Accordingly, in plasma from FD patients, the lipid-intermediate DG originating from peripheral lipolysis was reduced as well (Figure 6C). Overall, metabolomic and lipidomic data unveiled a deep difference in the metabolic profile of FD patients compared to healthy controls, most likely linked to the metabolic disarrangement of skeletal muscle with its reduced capability in using lipids as fuel.

mir-17 mediated upregulation of HIF-1α drives the metabolic disarrangement in FD

To explore the involvement of HIF-1α in the metabolic switch of FD muscle toward anaerobic glycolysis, we evaluated its levels in the skeletal muscle isolated from FD mice. HIF-1α levels were significantly upregulated in FD compared to WT muscle (Figure 7A).

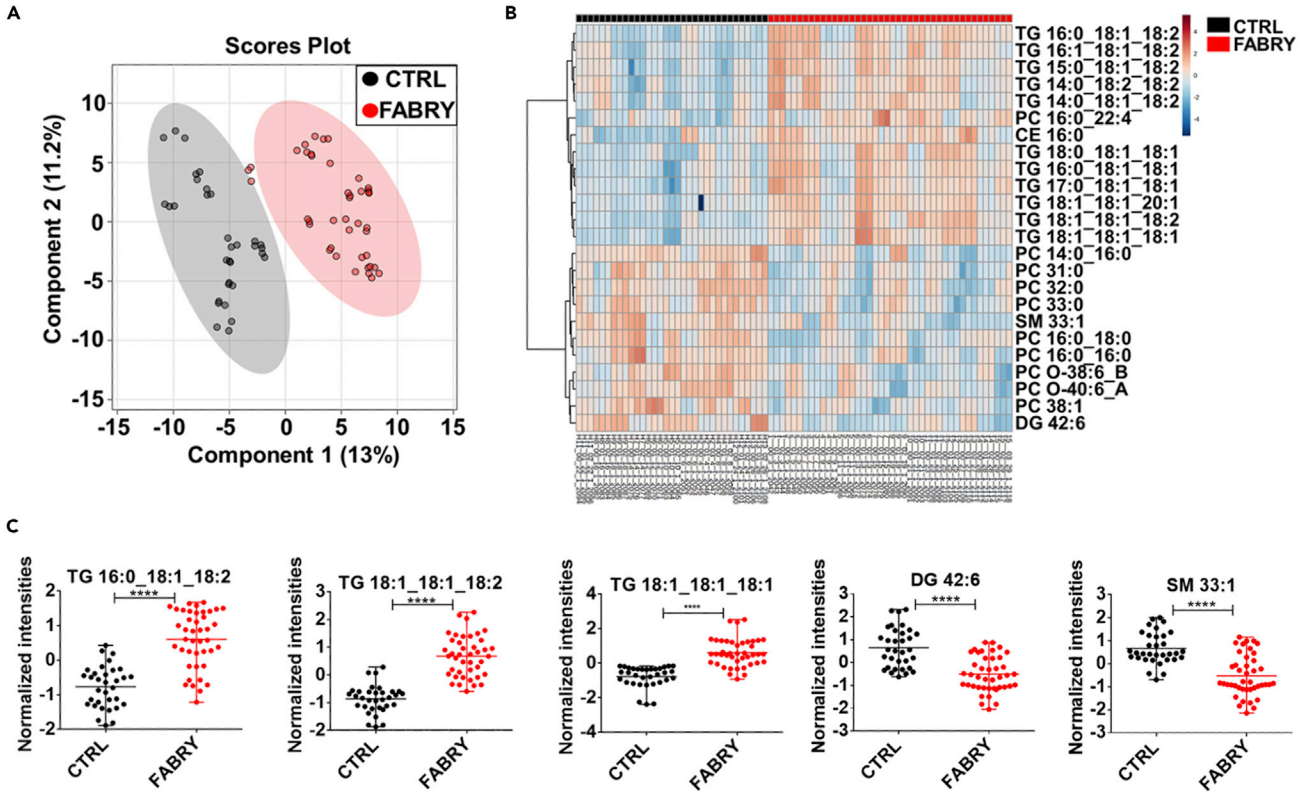

Figure 6. Lipidomic analysis was conducted on the hydrophobic fraction of plasma-derived from FD and healthysubjects by UHPLC-TIMS-qTOF mass spectrometry.

Two dimensional Partial least squares-discriminant analysis (PLS-DA) score plots (A) of lipidome analysis determined using UHPLC-HRMS showing clustering and separation between Controls (black) and FD (red) groups. (B) Heatmap of top statistically relevant lipids ($p < 0.05$, FDR< 0.01), (C) normalized intensity of statistically relevant lipids (TG: triacylglycerol, SM: sphingomyelin, DG: diacylglycerol). Data are represented as mean ± SD; *t* test: ****p <0.0001.

In cells obtained from FD patients, the upregulation of HIF-1α was significant as well (Figure 7B), suggesting its functional role in determining the contextual high expression of glycolytic enzymes detected in FD cells (see Figure4, panels EF). Consistently, when we silenced HIF-1 in FD cells, the highly expressed glycolytic enzymes HK and PDK1 were downregulated, confirming that HIF-1α is responsible for the hyperactivation of the glycolytic machinery in FD cells (Figure S2A).

The evidence of high levels HIF-1α levels even in cultured human fibroblasts supports a hypoxia-independent stabilization of HIF-1α in FD. The regulation of Prolyl Hydroxylase 2 (PHD2)/HIF-1α levels by miR-17 is among the non-canonical hypoxia-driven pathways of HIF-1α activation; specifically, PHD2 is physiologically deputed to hydroxylation mediated HIF-1α degradation, and miR-17 is reported to downregulate PHD2 determining HIF-1 accumulation.[39] As we previously described, miR-17 is upregulated in FD patients.[27] Accordingly, we confirmed the higher levels of miR-17 in FD population as well as in FD mice compared to control groups (Figures 7C and 7D). Consistent with our hypothesis of miR-17-mediated PHD2 downregulation in FD, we found reduced PHD2 levels in FD cells compared to control cells (Figure S2B).

To mechanistically demonstrate that miR-17 is responsible for HIF-1α upregulation in FD cells, we employed a specific antagomir targeting miR-17 (AntagomiR-17). The treatment with antagomiR-17 significantly reduced HIF-1α levels in FD cells (Figure 7E), while determining an increase of PHD2 levels (Figure S2C). Accordingly, the enzymes supporting the high glycolytic rate, HKII and PDK1, were significantly downregulated in FD cells treated with antagomiR-17 (Figure 7F), as well as glucose consumption and lactate production (Figures S2D and S2E). These results demonstrate the role of miR-17/PHD2/HIF-1 axis as the key mechanism for the metabolic switch occurring in FD cells.

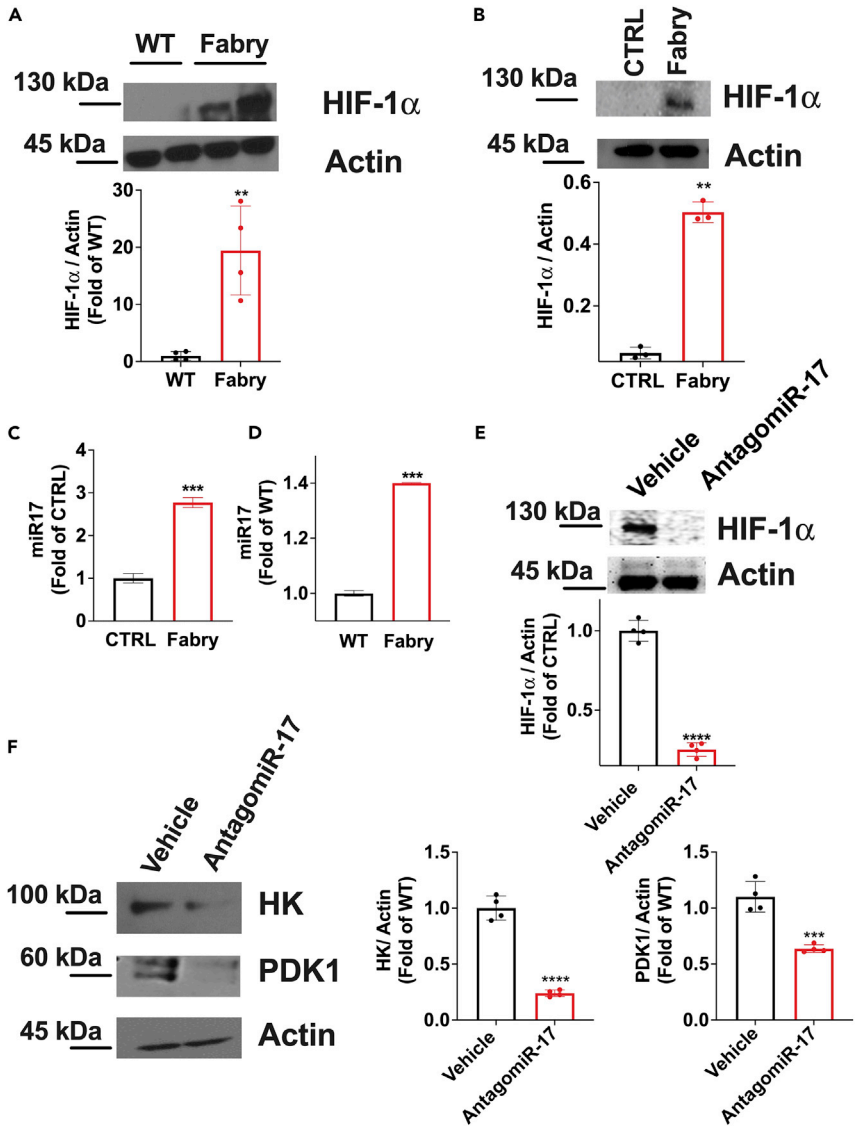

Figure 7. Immunoblot analysis and detection of HIF-1α on whole muscle lysate and on FD-patients derived fibroblasts (A,B respectively), with actin levels used as loading control.

miR-17 levels were detected in plasma from patients (FD vs healthy controls) and from mice (FD vs Wildtype) (C,D). Fibroblasts from FD patients were transfected with 30 nM of control antgomiR (CTRL) or with 30 nM of AntagomiR-17. Western blot analysis was performed to detect the effects of AntagomiR-17 treatment on HIF-1α (E), HK and PDK1 levels (F). The pictures are representative of 3 independent experiments. Data are represented as mean ± SEM; *t* test: **p <0.005, ***p <0.0005, ****p <0.0001 Fabry versus CTRL (A-B-C-D), antagomiR versus Vehicle (E-F).

DISCUSSION

To the best of our knowledge, this study is the first to comprehensively investigate the muscular phenotype in FD. In both FD patients and in our mouse model, we show a metabolic switch toward anaerobic metabolism, as demonstrated by the accumulation of fatty acids as underutilized metabolites, and lactates as overproduced catabolites. We identified in the normoxic HIF-1α upregulation mediated by miR-17 the mechanistic trigger of these metabolic alterations.

The involvement of skeletal muscle in FD is testified by muscular cramps and pain often reported by young patients, which eventually evolve toward fatigability, asthenia, and reduced motion in the advanced stages of the disease,[9] with significant impact on quality of life.[48–52] Nevertheless, skeletal muscle research in FD

has been enduringly neglected. Skeletal muscle performance is known to depend on many physiological determinants.[53] Here, we focused on metabolic alterations. Our mouse model of FD shows an altered composition of muscle fibers. Pathological conditions can affect muscle fibers' composition, impacting exercise tolerance and susceptibility to fatigue.[54–56] The increased abundance of fast/glycolytic fibers in FD muscle, accompanied by a relative reduction of slow fibers, highlights a compromised oxidative capacity and explains the higher power output and susceptibility to fatigue of FD muscle. The upregulation of key enzymes regulating anaerobic glycolysis (HK, PDK1, LDH) confirms that FD muscle undergoes a metabolic remodeling, with expression of the biochemical machinery supporting lactacid metabolism. Accordingly, in FD mice we observed resting intramuscular lactate accumulation and stress-induced lactate over-production, ratifying that during exercise the muscle work is supported by anaerobic glycolysis.

Strikingly, having observed exercise intolerance and stress-induced lactate accumulation in FD patients is in line with the metabolic disarrangement detected in mice. Similarly, patient-derived fibroblasts exhibited an upregulation of the same enzymes detected in the muscle of FD mice, corroborating the prevalent glycolytic metabolism. Our findings are therefore clearly translational, as they are observed both in FD mice and humans. The data obtained from FD patients-derived cells *in vitro*, show that the anaerobic energetic metabolism is common to different cell types in FD, ruling out the influence of confounding factors like sedentarity and atrophy.[57] It also proves that metabolic disarrangements in FD are genetically determined, rather than being dependent on cell types and environment. In this scenario, exercise testing and relative blood lactate detection should be considered relevant for the monitoring of FD onset and progression.

Bracing this view, we showed that FD treatment can ameliorate impaired exercise tolerance in patients. So, exercise intolerance could represent a further parameter to rely on for starting and monitoring treatment, with the canonical parameters of use in clinical practice.

Further evidence of altered energetic metabolism attained from the analysis of plasma lipidic metabolites. FD patients accumulate triglycerides (TGs). Because the muscle is one of the most important energivorous tissues in the body, it is conceivable to consider the inadequate consumption of triglycerides prevalently owing to muscle metabolism. Indeed, a similar pattern of plasma lipid abnormalities is described for primitive myopathies, like Becker and Duchenne dystrophies,[46] where the increase in circulating TGs is again accounted for by the reduced capability of the muscle to utilize lipids.[47] Also, the reduced expression of acylcarnitines further supports the reduction of fatty acids as an energetic substrate in mitochondria. Overall, the metabolic profile of FD muscle is similar to the one reported in genetic myopathies characterized by an increased rate of glycolysis with exercise intolerance, blood lactate accumulation, and reduction of circulating acylcarnitines.[58] In this framework, FD can be considered a metabolic myopathy itself. Another feature that FD has in common with myopathies is the upregulation of HIF-1.[29] Indeed, an activation of HIF-1 – which is in turn responsible for triggering an upregulation of the enzymes supporting the glycolytic metabolic switch – has been described in several myopathies including Duchenne and Becker.

Consistently, HIF-1α is upregulated also in cells from FD patients, contextually to the key enzymes of glycolysis. In accordance with these findings, the HIF-1α inactivation in FD cells induced a significant downregulation of the main glycolytic enzymes, proving that HIF-1 is the master regulator of metabolic switch in FD.

The *in vitro* HIF-1α accumulation and the relative upregulation of glycolysis, in FD cells cultured in normoxic conditions, demonstrate that the HIF-1 mediated metabolic switch is independent from hypoxia. Rather, a Warburg effect is occurring, similar to the one described in muscle dystrophies.[29] This non-canonical HIF-1α activation, not controlled by hypoxia, is likely dependent on the intrinsic metabolic stress occurring in FD cells.[25,59] We recently demonstrated in FD patients an increased expression of specific miRs that are considered mitochondrial and metabolic stress markers, including miR-17.[27] Recent evidence shows that miR-17 increases in response to different forms of cellular stress, including nutrient deprivation,[60] and acts as a key mediator of metabolic reprogramming.[40] Moreover, miR-17 has been reported to directly target PDH2 causing HIF-1α stabilization.[39] Indeed, in FD, we contextually observed miR-17 and HIF-1 upregulation alongside PHD2 downregulation, supporting the view that miR-17-mediated PHD2 reduction represents a mechanism of non-canonical HIF-1α accumulation and metabolic reprogramming in FD cells. Here, we demonstrated for the first time the functional involvement of the miR-17/HIF-1α pathway as the main responsible for metabolic disarrangement in FD. Indeed, antagomiR-17 is not only able to increase

PHD2 and to abrogate HIF-1 accumulation, but also to prevent the metabolic remodeling by reducing the expression of the main glycolytic enzymes, diminishing glucose consumption and lactate production.

Beyond the FD context, our findings unveil a novel mechanism by which miR-17 ensures the Warburg effect, which could be potentially extended to other pathological conditions. Emerging evidence shows that the Warburg effect plays an essential role in non-tumor diseases, including cardiac hypertrophy, heart failure, diabetes, atherosclerosis, Alzheimer's disease, and multiple sclerosis.[61] Of interest, in many of these disorders, like for heart failure and diabetic cardiomyopathy, augmented miR-17 levels have been reported,[62,63] as well as altered muscular capacity and exercise tolerance.

Therefore, we can speculate that the miR-17-dependent Warburg effect could represent a new potential therapeutic target for FD and many other pathological conditions beyond FD, including chronic diseases in which musculoskeletal manifestations impact patients' quality of like. In this view, our finding opens new research horizons.

Conclusions

We unveiled a metabolic remodeling of FD skeletal muscle, resembling the Warburg Effect observed in genetic myopathies. In FD, the "aerobic glycolysis" is supported by HIF-1, whose accumulation is hypoxia-independent and mediated by miR-17 upregulation. Blood lactate emerged as a powerful biosensor of this metabolic disarrangement representing a new potential diagnostic and monitoring tool.

Overall, our findings place FD in a new light, featuring characteristics that are often detected in genetic myopathies. Also, they indicate the relevance of the muscular phenotype characterization in FD patients, for which the miR-17/HIF-1 pathway could represent a new therapeutic target. Our results can be extended to other conditions in which the miR-17/HIF-1 pathway is potentially altered, including cardiac hypertrophy and diabetic cardiomyopathy.[62,63]

Limitations of the study

In the present study we did not evaluate the impact of the different FD related mutations on muscle phenotype, metabolism, and energetic alterations. Furthermore, the impact of the therapy on exercise tolerance has been evaluated in a very small pool of FD patients. A clinical trial of naive FD patients evaluated with longer follow-up is warranted to confirm that exercise tolerance testing can help stratifying FD progression and monitor the response to therapy in FD patients.

STAR★METHODS

Detailed methods are provided in the online version of this paper and include the following:

- KEY RESOURCES TABLE
- RESOURCE AVAILABILITY
  - Lead contact
  - Material availability
  - Data and code availability
- EXPERIMENTAL MODEL AND SUBJECT DETAILS
  - Human study population
  - Animals
  - Cell culture
- METHOD DETAILS
  - Determination of exercise tolerance in patients
  - Plasma metabolome and lipidome extraction
  - FIA-FT-ICR metabolome analysis
  - RP-UHPLC-TIMS-MS lipidome analysis
  - HRMS data analysis and processing
  - Detection of miR-17 levels
  - Spontaneous activity recording
  - Weight test
  - Glucose tolerance test
  - Muscle dissection and protein extraction

- Immunofluorescence on muscle tissue
- Intramuscolar lactate determination
- HIF-1 siRNA and AntagomiR-17 transfection
- *In vitro* evaluation of glucose consumption and lactate production
- Assessment of extracellular acidification rate (ECAR)
- Western blot analysis
- Real-time PCR

● QUANTIFICATION AND STATISTICAL ANALYSIS

SUPPLEMENTAL INFORMATION

Supplemental information can be found online at https://doi.org/10.1016/j.isci.2023.106074.

ACKNOWLEDGMENTS

We thank the trainees of the Sport Medicine School and of Urgent Medicine School, Dr. Luca Allocca, Dr. Giada Annarumma, Dr. Amos Cocola, Dr. Rosita Mottola, Dr. Vincenza Notarangelo, Dr. Pasquale Perrella, Dr. Marco Rumolo, and Dr. Roberto Bianco, as well as Dr. Paola Nesci for her secretarial support. We thank Dr. Desnick for kindly providing us with the founders and Dr. Jankauskas for technical assistance and helpful discussions. GI is supported by a grant from the Italian Ministry of Research (PRIN-2017HTKLRF) and Campania Bioscience (PON03PE_00060_8). DS is supported by Finanziamento della Ricerca di Ateneo of Federico II University (FRA 54 2020). JG is supported by PON "REACT-EU" IV.4 action 2014–2020. GS is supported in part by the National Institutes of Health (*NIH*): National Heart, Lung, and Blood Institute (*NHLBI*: R01-HL164772, R01-HL159062, R01-HL146691, T32-HL144456), National Institute of Diabetes and Digestive and Kidney Diseases (*NIDDK*: R01-DK123259, R01-DK033823), National Center for Advancing Translational Sciences (*NCATS*: UL1TR002556-06), by the Diabetes Action Research and Education Foundation, and by the Monique Weill-Caulier and Irma T. Hirschl Trusts.

AUTHOR CONTRIBUTIONS

Methodology: J.G., D.S., and G.I.; investigation: J.G., A.F., F.C., A.B., R.A., A.V., E.S., F.M., E.S., V.D.A., S.P., A.B., L.S., E.D.V., A.P., E.R., T.D.R., G.S., and D.S.; validation: J.G., A.F., F.C., R.A., P.C., and M.C.; formal analysis: J.G., E.S., D.S., M.C., P.C., A.C., A.P., G.S., and G.I.; data curation: J.G., G.S., D.S., and G.I.; writing – original draft: J.G. and D.S.; writing – review and editing: G.S., D.S., A.P., and G.I. All authors read and approved the final version of the manuscript.

DECLARATION OF INTERESTS

The authors have declared that no conflict of interest exists.

Received: October 20, 2022
Revised: December 19, 2022
Accepted: January 24, 2023
Published: January 27, 2023

REFERENCES

1. Eng, C.M., Germain, D.P., Banikazemi, M., Warnock, D.G., Wanner, C., Hopkin, R.J., Bultas, J., Lee, P., Sims, K., Brodie, S.E., et al. (2006). Fabry disease: guidelines for the evaluation and management of multi-organ system involvement. Genet. Med. *8*, 539–548. https://doi.org/10.1097/01.gim.0000237866.70357.c6.

2. Orsborne, C., Bradley, J., Bonnett, L.J., Pleva, L.A., Naish, J.H., Clark, D.G., Abidin, N., Woolfson, P., Nucifora, G., Schmitt, M., et al. (2022). Validated model for prediction of adverse cardiac outcome in patients with Fabry disease. J. Am. Coll. Cardiol. *80*, 982–994. https://doi.org/10.1016/j.jacc.2022.06.022.

3. Pisani, A., Visciano, B., Imbriaco, M., Di Nuzzi, A., Mancini, A., Marchetiello, C., and Riccio, E. (2014). The kidney in Fabry's disease. Clin. Genet. *86*, 301–309. https://doi.org/10.1111/cge.12386.

4. Alfen, F., Putscher, E., Hecker, M., Zettl, U.K., Hermann, A., and Lukas, J. (2022). Abnormal pre-mRNA splicing in exonic Fabry disease-causing GLA mutations. Int. J. Mol. Sci. *23*, 15261. https://doi.org/10.3390/ijms232315261.

5. Germain, D.P., Shabbeer, J., Cotigny, S., and Desnick, R.J. (2002). Fabry disease: twenty novel alpha-galactosidase A mutations and genotype-phenotype correlations in classical and variant phenotypes. Mol. Med. *8*, 306–312.

6. Topaloglu, A.K., Ashley, G.A., Tong, B., Shabbeer, J., Astrin, K.H., Eng, C.M., and Desnick, R.J. (1999). Twenty novel mutations in the alpha-galactosidase A gene causing Fabry disease. Mol. Med. *5*, 806–811.

7. Pihlstrøm, H.K., Weedon-Fekjær, M.S., Bjerkely, B.L., von der Lippe, C., Ørstavik, K., Mathisen, P., Heimdal, K., Jenssen, T.G., Dahle, D.O., Solberg, O.K., and Sigurdardottir, S. (2021). Health-related quality of life in Norwegian adults with Fabry

disease: disease severity, pain, fatigue and psychological distress. JIMD Rep. *62*, 56–69. https://doi.org/10.1002/jmd2.12240.

8. Rob, D., Marek, J., Dostalova, G., and Linhart, A. (2022). Heart failure in Fabry disease revisited: application of current heart failure guidelines and recommendations. ESC Heart Fail. *9*, 4043–4052. https://doi.org/10.1002/ehf2.14091.

9. Chimenti, C., Padua, L., Pazzaglia, C., Morgante, E., Centurion, C., Antuzzi, D., Russo, M.A., and Frustaci, A. (2012). Cardiac and skeletal myopathy in Fabry disease: a clinicopathologic correlative study. Hum. Pathol. *43*, 1444–1452. https://doi.org/10.1016/j.humpath.2011.09.020.

10. Graziani, F., Lillo, R., Panaioli, E., Spagnoletti, G., Pieroni, M., Ferrazzi, P., Camporeale, A., Verrecchia, E., Sicignano, L.L., Manna, R., and Crea, F. (2021). Evidence of evolution towards left midventricular obstruction in severe Anderson-Fabry cardiomyopathy. ESC Heart Fail. *8*, 725–728. https://doi.org/10.1002/ehf2.13101.

11. Duning, T., Deppe, M., Keller, S., Schiffbauer, H., Stypmann, J., Böntert, M., Schaefer, R., and Young, P. (2009). Excessive daytime sleepiness is a common symptom in Fabry disease. Case Rep. Neurol. *1*, 33–40. https://doi.org/10.1159/000226792.

12. Üçeyler, N., Magg, B., Thomas, P., Wiedmann, S., Heuschmann, P., and Sommer, C. (2014). A comprehensive Fabry-related pain questionnaire for adult patients. Pain *155*, 2301–2305. https://doi.org/10.1016/j.pain.2014.08.024.

13. MacDermot, K.D., Holmes, A., and Miners, A.H. (2001). Anderson-Fabry disease: clinical manifestations and impact of disease in a cohort of 98 hemizygous males. J. Med. Genet. *38*, 750–760. https://doi.org/10.1136/jmg.38.11.750.

14. Laney, D.A., Peck, D.S., Atherton, A.M., Manwaring, L.P., Christensen, K.M., Shankar, S.P., Grange, D.K., Wilcox, W.R., and Hopkin, R.J. (2015). Fabry disease in infancy and early childhood: a systematic literature review. Genet. Med. *17*, 323–330. https://doi.org/10.1038/gim.2014.120.

15. Bouwman, M.G., Maurice-Stam, H., Linthorst, G.E., Hollak, C.E.M., Wijburg, F.A., and Grootenhuis, M.A. (2011). Impact of growing up with Fabry disease on achievement of psychosocial milestones and quality of life. Mol. Genet. Metab. *104*, 308–313. https://doi.org/10.1016/j.ymgme.2011.07.006.

16. Schmitz, B., Thorwesten, L., Lenders, M., Duning, T., Stypmann, J., Brand, E., and Brand, S.M. (2016). Physical exercise in patients with Fabry disease - a pilot study. Int. J. Sports Med. *37*, 1066–1072. https://doi.org/10.1055/s-0042-110205.

17. Tomé, F.M., Fardeau, M., and Lenoir, G. (1977). Ultrastructure of muscle and sensory nerve in Fabry's disease. Acta Neuropathol. *38*, 187–194. https://doi.org/10.1007/BF00688064.

18. Uchino, M., Uyama, E., Kawano, H., Hokamaki, J., Kugiyama, K., Murakami, Y., Yasue, H., and Ando, M. (1995). A histochemical and electron microscopic study of skeletal and cardiac muscle from a Fabry disease patient and carrier. Acta Neuropathol. *90*, 334–338. https://doi.org/10.1007/BF00296520.

19. Lidove, O., Zeller, V., Chicheportiche, V., Meyssonnier, V., Sené, T., Godot, S., and Ziza, J.M. (2016). Musculoskeletal manifestations of Fabry disease: a retrospective study. Joint Bone Spine *83*, 421–426. https://doi.org/10.1016/j.jbspin.2015.11.001.

20. Wagner, M., Krämer, J., Blohm, E., Vergho, D., Weidemann, F., Breunig, F., and Wanner, C. (2014). Kidney function as an underestimated factor for reduced health related quality of life in patients with Fabry disease. BMC Nephrol. *15*, 188. https://doi.org/10.1186/1471-2369-15-188.

21. Sorriento, D., and Iaccarino, G. (2021). The cardiovascular phenotype in Fabry disease: new findings in the research field. Int. J. Mol. Sci. *22*, 1331. https://doi.org/10.3390/ijms22031331.

22. Janssen, I., Heymsfield, S.B., Wang, Z.M., and Ross, R. (2000). Skeletal muscle mass and distribution in 468 men and women aged 18-88 yr. J. Appl. Physiol. *89*, 81–88. https://doi.org/10.1152/jappl.2000.89.1.81.

23. Zurlo, F., Nemeth, P.M., Choksi, R.M., Sesodia, S., and Ravussin, E. (1994). Whole-body energy metabolism and skeletal muscle biochemical characteristics. Metabolism *43*, 481–486. https://doi.org/10.1016/0026-0495(94)90081-7.

24. Pellissier, J.F., Van Hoof, F., Bourdet-Bonerandi, D., Monier-Faugere, M.C., and Toga, M. (1981). Morphological and biochemical changes in muscle and peripheral nerve in Fabry's disease. Muscle Nerve *4*, 381–387. https://doi.org/10.1002/mus.880040506.

25. Lücke, T., Höppner, W., Schmidt, E., Illsinger, S., and Das, A.M. (2004). Fabry disease: reduced activities of respiratory chain enzymes with decreased levels of energy-rich phosphates in fibroblasts. Mol. Genet. Metab. *82*, 93–97. https://doi.org/10.1016/j.ymgme.2004.01.011.

26. Berardo, A., DiMauro, S., and Hirano, M. (2010). A diagnostic algorithm for metabolic myopathies. Curr. Neurol. Neurosci. Rep. *10*, 118–126. https://doi.org/10.1007/s11910-010-0096-4.

27. Gambardella, J., Fiordelisi, A., Sorriento, D., Cerasuolo, F., Buonaiuto, A., Avvisato, R., Pisani, A., Varzideh, F., Riccio, E., Santulli, G., and Iaccarino, G. (2023). Mitochondrial microRNAs are dysregulated in patients with Fabry Disease. J. Pharmacol. Exp. Ther. *384*, 72–78. https://doi.org/10.1124/jpet.122.001250.

28. Ravarotto, V., Carraro, G., Pagnin, E., Bertoldi, G., Simioni, F., Maiolino, G., Martinato, M., Landini, L., Davis, P.A., and Calò, L.A. (2018). Oxidative stress and the altered reaction to it in Fabry disease: a possible target for cardiovascular-renal remodeling? PLoS One *13*, e0204618. https://doi.org/10.1371/journal.pone.0204618.

29. Nguyen, T.H., Conotte, S., Belayew, A., Declèves, A.E., Legrand, A., and Tassin, A. (2021). Hypoxia and hypoxia-inducible factor signaling in muscular dystrophies: cause and consequences. Int. J. Mol. Sci. *22*, 7220. https://doi.org/10.3390/ijms22137220.

30. Seagroves, T.N., Ryan, H.E., Lu, H., Wouters, B.G., Knapp, M., Thibault, P., Laderoute, K., and Johnson, R.S. (2001). Transcription factor HIF-1 is a necessary mediator of the pasteur effect in mammalian cells. Mol. Cell Biol. *21*, 3436–3444. https://doi.org/10.1128/MCB.21.10.3436-3444.2001.

31. Favier, F.B., Britto, F.A., Freyssenet, D.G., Bigard, X.A., and Benoit, H. (2015). HIF-1-driven skeletal muscle adaptations to chronic hypoxia: molecular insights into muscle physiology. Cell. Mol. Life Sci. *72*, 4681–4696. https://doi.org/10.1007/s00018-015-2025-9.

32. He, W., Batty-Stuart, S., Lee, J.E., and Ohh, M. (2021). HIF-1alpha hydroxyprolines modulate oxygen-dependent protein stability via single VHL interface with comparable effect on ubiquitination rate. J. Mol. Biol. *433*, 167244. https://doi.org/10.1016/j.jmb.2021.167244.

33. Kanemaru, H., Mizukami, Y., Kaneko, A., Tagawa, H., Kimura, T., Kuriyama, H., Sawamura, S., Kajihara, I., Makino, K., Miyashita, A., et al. (2021). A mechanism of cooling hot tumors: lactate attenuates inflammation in dendritic cells. iScience *24*, 103067. https://doi.org/10.1016/j.isci.2021.103067.

34. Déry, M.A.C., Michaud, M.D., and Richard, D.E. (2005). Hypoxia-inducible factor 1: regulation by hypoxic and non-hypoxic activators. Int. J. Biochem. Cell Biol. *37*, 535–540. https://doi.org/10.1016/j.biocel.2004.08.012.

35. Iommarini, L., Porcelli, A.M., Gasparre, G., and Kurelac, I. (2017). Non-canonical mechanisms regulating hypoxia-inducible factor 1 alpha in cancer. Front. Oncol. *7*, 286. https://doi.org/10.3389/fonc.2017.00286.

36. Zhang, Y., Zhai, Z., Duan, J., Wang, X., Zhong, J., Wu, L., Li, A., Cao, M., Wu, Y., Shi, H., et al. (2022). Lactate: the mediator of metabolism and immunosuppression. Front. Endocrinol. *13*, 901495. https://doi.org/10.3389/fendo.2022.901495.

37. Abdel-Haleem, A.M., Lewis, N.E., Jamshidi, N., Mineta, K., Gao, X., and Gojobori, T. (2017). The emerging facets of non-cancerous Warburg effect. Front. Endocrinol. *8*, 279. https://doi.org/10.3389/fendo.2017.00279.

38. Deng, P., Li, K., Gu, F., Zhang, T., Zhao, W., Sun, M., and Hou, B. (2021). LINC00242/miR-1-3p/G6PD axis regulates Warburg effect and affects gastric cancer proliferation and apoptosis. Mol. Med. *27*, 9. https://doi.org/10.1186/s10020-020-00259-y.

39. Chen, T., Zhou, Q., Tang, H., Bozkanat, M., Yuan, J.X.J., Raj, J.U., and Zhou, G. (2016). miR-17/20 controls Prolyl hydroxylase 2 (PHD2)/Hypoxia-Inducible factor 1 (HIF1) to

regulate pulmonary artery smooth muscle cell proliferation. J. Am. Heart Assoc. *5*, e004510. https://doi.org/10.1161/JAHA.116.004510.

40. Izreig, S., Samborska, B., Johnson, R.M., Sergushichev, A., Ma, E.H., Lussier, C., Loginicheva, E., Donayo, A.O., Poffenberger, M.C., Sagan, S.M., et al. (2016). The miR-17 approximately 92 microRNA cluster is a global regulator of tumor metabolism. Cell Rep. *16*, 1915–1928. https://doi.org/10.1016/j.celrep.2016.07.036.

41. Luo, F., Li, Y., Yuan, F., and Zuo, J. (2019). Hexokinase II promotes the Warburg effect by phosphorylating alpha subunit of pyruvate dehydrogenase. Chin. J. Cancer Res. *31*, 521–532. https://doi.org/10.21147/j.issn.1000-9604.2019.03.14.

42. Coburn, C.T., Knapp, F.F., Jr., Febbraio, M., Beets, A.L., Silverstein, R.L., and Abumrad, N.A. (2000). Defective uptake and utilization of long chain fatty acids in muscle and adipose tissues of CD36 knockout mice. J. Biol. Chem. *275*, 32523–32529. https://doi.org/10.1074/jbc.M003826200.

43. De Rosa, M., Gambardella, J., Shu, J., and Santulli, G. (2018). Dietary fat is a key determinant in balancing mitochondrial dynamics in heart failure: a novel mechanism underlying the obesity paradox. Cardiovasc. Res. *114*, 925–927. https://doi.org/10.1093/cvr/cvy074.

44. Morifuji, M., Sakai, K., Sanbongi, C., and Sugiura, K. (2005). Dietary whey protein downregulates fatty acid synthesis in the liver, but upregulates it in skeletal muscle of exercise-trained rats. Nutrition *21*, 1052–1058. https://doi.org/10.1016/j.nut.2005.01.010.

45. Perreault, L., Starling, A.P., Glueck, D., Brozinick, J.T., Sanders, P., Siddall, P., Kuo, M.S., Dabelea, D., and Bergman, B.C. (2016). Biomarkers of ectopic fat deposition: the next frontier in serum lipidomics. J. Clin. Endocrinol. Metab. *101*, 176–182. https://doi.org/10.1210/jc.2015-3213.

46. White, Z., Hakim, C.H., Theret, M., Yang, N.N., Rossi, F., Cox, D., Francis, G.A., Straub, V., Selby, K., Panagiotopoulos, C., et al. (2020). High prevalence of plasma lipid abnormalities in human and canine Duchenne and Becker muscular dystrophies depicts a new type of primary genetic dyslipidemia. J. Clin. Lipidol. *14*, 459–469.e0. https://doi.org/10.1016/j.jacl.2020.05.098.

47. Milad, N., White, Z., Tehrani, A.Y., Sellers, S., Rossi, F.M.V., and Bernatchez, P. (2017). Increased plasma lipid levels exacerbate muscle pathology in the mdx mouse model of Duchenne muscular dystrophy. Skelet. Muscle *7*, 19. https://doi.org/10.1186/s13395-017-0135-9.

48. Weidemann, F., Breunig, F., Beer, M., Sandstede, J., Turschner, O., Voelker, W., Ertl, G., Knoll, A., Wanner, C., and Strotmann, J.M. (2003). Improvement of cardiac function during enzyme replacement therapy in patients with Fabry disease: a prospective strain rate imaging study. Circulation *108*, 1299–1301. https://doi.org/10.1161/01.CIR.0000091253.71282.04.

49. Lobo, T., Morgan, J., Bjorksten, A., Nicholls, K., Grigg, L., Centra, E., and Becker, G. (2008). Cardiovascular testing in Fabry disease: exercise capacity reduction, chronotropic incompetence and improved anaerobic threshold after enzyme replacement. Intern. Med. J. *38*, 407–414. https://doi.org/10.1111/j.1445-5994.2008.01669.x.

50. Lenders, M., Stypmann, J., Duning, T., Schmitz, B., Brand, S.M., and Brand, E. (2016). Serum-mediated inhibition of enzyme replacement therapy in Fabry disease. J. Am. Soc. Nephrol. *27*, 256–264. https://doi.org/10.1681/ASN.2014121226.

51. Politei, J.M., Bouhassira, D., Germain, D.P., Goizet, C., Guerrero-Sola, A., Hilz, M.J., Hutton, E.J., Karaa, A., Liguori, R., Üçeyler, N., et al. (2016). Pain in Fabry disease: practical recommendations for diagnosis and treatment. CNS Neurosci. Ther. *22*, 568–576. https://doi.org/10.1111/cns.12542.

52. Kritzer, A., Siddharth, A., Leestma, K., and Bodamer, O. (2019). Early initiation of enzyme replacement therapy in classical Fabry disease normalizes biomarkers in clinically asymptomatic pediatric patients. Mol. Genet. Metab. Rep. *21*, 100530. https://doi.org/10.1016/j.ymgmr.2019.100530.

53. van der Zwaard, S., Brocherie, F., and Jaspers, R.T. (2021). Under the hood: skeletal muscle determinants of endurance performance. Front. Sports Act. Living *3*, 719434. https://doi.org/10.3389/fspor.2021.719434.

54. Chaillou, T. (2018). Skeletal muscle fiber type in hypoxia: adaptation to high-altitude exposure and under conditions of pathological hypoxia. Front. Physiol. *9*, 1450. https://doi.org/10.3389/fphys.2018.01450.

55. Fitts, R.H., and Widrick, J.J. (1996). Muscle mechanics: adaptations with exercise-training. Exerc. Sport Sci. Rev. *24*, 427–473.

56. Venhoff, N., Lebrecht, D., Pfeifer, D., Venhoff, A.C., Bissé, E., Kirschner, J., and Walker, U.A. (2012). Muscle-fiber transdifferentiation in an experimental model of respiratory chain myopathy. Arthritis Res. Ther. *14*, R233. https://doi.org/10.1186/ar4076.

57. Stein, T.P., and Wade, C.E. (2005). Metabolic consequences of muscle disuse atrophy. J. Nutr. *135*, 1824S–1828S. https://doi.org/10.1093/jn/135.7.1824S.

58. Das, A.M., Steuerwald, U., and Illsinger, S. (2010). Inborn errors of energy metabolism associated with myopathies. J. Biomed. Biotechnol. *2010*, 340849. https://doi.org/10.1155/2010/340849.

59. Marino, S., Borsini, W., Buchner, S., Mortilla, M., Stromillo, M.L., Battaglini, M., Giorgio, A., Bramanti, P., Federico, A., and De Stefano, N. (2006). Diffuse structural and metabolic brain changes in Fabry disease. J. Neurol. *253*, 434–440. https://doi.org/10.1007/s00415-005-0020-z.

60. Li, H., and Yang, B.B. (2012). Stress response of glioblastoma cells mediated by miR-17-5p targeting PTEN and the passenger strand miR-17-3p targeting MDM2. Oncotarget *3*, 1653–1668. https://doi.org/10.18632/oncotarget.810.

61. Chen, Z., Liu, M., Li, L., and Chen, L. (2018). Involvement of the Warburg effect in non-tumor diseases processes. J. Cell. Physiol. *233*, 2839–2849. https://doi.org/10.1002/jcp.25998.

62. Kansakar, U., Varzideh, F., Mone, P., Jankauskas, S.S., and Santulli, G. (2022). Functional role of microRNAs in regulating cardiomyocyte death. Cells *11*, 983. https://doi.org/10.3390/cells11060983.

63. Danielson, L.S., Park, D.S., Rotllan, N., Chamorro-Jorganes, A., Guijarro, M.V., Fernandez-Hernando, C., Fishman, G.I., Phoon, C.K.L., and Hernando, E. (2013). Cardiovascular dysregulation of miR-17-92 causes a lethal hypertrophic cardiomyopathy and arrhythmogenesis. FASEB J *27*, 1460–1467. https://doi.org/10.1096/fj.12-221994.

64. Schneider, C.A., Rasband, W.S., and Eliceiri, K.W. (2012). NIH Image to ImageJ: 25 years of image analysis. Nat. Methods *9*, 671–675. https://doi.org/10.1038/nmeth.2089.

65. Vardarli, I., Rischpler, C., Herrmann, K., and Weidemann, F. (2020). Diagnosis and screening of patients with Fabry disease. Ther. Clin. Risk Manag. *16*, 551–558. https://doi.org/10.2147/TCRM.S247814.

66. Parisi, S., Polishchuk, E.V., Allocca, S., Ciano, M., Musto, A., Gallo, M., Perone, L., Ranucci, G., Iorio, R., Polishchuk, R.S., and Bonatti, S. (2018). Characterization of the most frequent ATP7B mutation causing Wilson disease in hepatocytes from patient induced pluripotent stem cells. Sci. Rep. *8*, 6247. https://doi.org/10.1038/s41598-018-24717-0.

67. Bruce, R.A., Blackmon, J.R., Jones, J.W., and Strait, G. (2004). Exercising testing in adult normal subjects and cardiac patients. Ann. Noninvasive Electrocardiol. *9*, 291–303. https://doi.org/10.1111/j.1542-474X.2004.93003.x.

68. Baker, J.S., Thomas, N., Cooper, S.M., Davies, B., and Robergs, R.A. (2012). Exercise duration and blood lactate concentrations following high intensity cycle ergometry. Res. Sports Med. *20*, 129–141. https://doi.org/10.1080/15438627.2012.634723.

69. Matyash, V., Liebisch, G., Kurzchalia, T.V., Shevchenko, A., and Schwudke, D. (2008). Lipid extraction by methyl-tert-butyl ether for high-throughput lipidomics. J. Lipid Res. *49*, 1137–1146. https://doi.org/10.1194/jlr.D700041-JLR200.

70. Vorkas, P.A., Isaac, G., Anwar, M.A., Davies, A.H., Want, E.J., Nicholson, J.K., and Holmes, E. (2015). Untargeted UPLC-MS profiling pipeline to expand tissue metabolome coverage: application to cardiovascular disease. Anal. Chem. *87*, 4184–4193. https://doi.org/10.1021/ac503775m.

71. Mone, P., Gambardella, J., Wang, X., Jankauskas, S.S., Matarese, A., and Santulli, G. (2021). miR-24 targets the transmembrane glycoprotein neuropilin-1 in human brain

microvascular endothelial cells. Noncoding. RNA *7*, 9. https://doi.org/10.3390/ncrna7010009.

72. Umanskaya, A., Santulli, G., Xie, W., Andersson, D.C., Reiken, S.R., and Marks, A.R. (2014). Genetically enhancing mitochondrial antioxidant activity improves muscle function in aging. Proc. Natl. Acad. Sci. USA. *111*, 15250–15255. https://doi.org/10.1073/pnas.1412754111.

73. Deacon, R.M. (2013). Measuring the strength of mice. J Vis Exp. https://doi.org/10.3791/2610.

74. Santulli, G., Pagano, G., Sardu, C., Xie, W., Reiken, S., D'Ascia, S.L., Cannone, M., Marziliano, N., Trimarco, B., Guise, T.A., et al. (2015). Calcium release channel RyR2 regulates insulin release and glucose homeostasis. J. Clin. Invest. *125*, 1968–1978. https://doi.org/10.1172/JCI79273.

75. Santulli, G., Lombardi, A., Sorriento, D., Anastasio, A., Del Giudice, C., Formisano, P., Béguinot, F., Trimarco, B., Miele, C., and Iaccarino, G. (2012). Age-related impairment in insulin release: the essential role of beta(2)-adrenergic receptor. Diabetes *61*, 692–701. https://doi.org/10.2337/db11-1027.

76. Fusco, A., Santulli, G., Sorriento, D., Cipolletta, E., Garbi, C., Dorn, G.W., 2nd, Trimarco, B., Feliciello, A., and Iaccarino, G. (2012). Mitochondrial localization unveils a novel role for GRK2 in organelle biogenesis. Cell. Signal. *24*, 468–475. https://doi.org/10.1016/j.cellsig.2011.09.026.

77. Cipolletta, E., Gambardella, J., Fiordelisi, A., Del Giudice, C., Di Vaia, E., Ciccarelli, M., Sala, M., Campiglia, P., Coscioni, E., Trimarco, B., et al. (2019). Antidiabetic and cardioprotective effects of pharmacological inhibition of GRK2 in db/db mice. Int. J. Mol. Sci. *20*, 1492. https://doi.org/10.3390/ijms20061492.

78. Gambardella, J., Sorriento, D., Bova, M., Rusciano, M., Loffredo, S., Wang, X., Petraroli, A., Carucci, L., Mormile, I., Oliveti, M., et al. (2020). Role of endothelial G protein-coupled receptor Kinase 2 in angioedema. Hypertension *76*, 1625–1636. https://doi.org/10.1161/HYPERTENSIONAHA.120.15130.

79. Yuan, Q., Yang, J., Santulli, G., Reiken, S.R., Wronska, A., Kim, M.M., Osborne, B.W., Lacampagne, A., Yin, Y., and Marks, A.R. (2016). Maintenance of normal blood pressure is dependent on IP3R1-mediated regulation of eNOS. Proc. Natl. Acad. Sci. USA. *113*, 8532–8537. https://doi.org/10.1073/pnas.1608859113.

80. Ciccarelli, M., Rusciano, M.R., Sorriento, D., Basilicata, M.F., Santulli, G., Campiglia, P., Bertamino, A., De Luca, N., Trimarco, B., Iaccarino, G., and Illario, M. (2014). CaMKII protects MKP-1 from proteasome degradation in endothelial cells. Cell. Signal. *26*, 2167–2174. https://doi.org/10.1016/j.cellsig.2014.06.009.

81. Morelli, M.B., Shu, J., Sardu, C., Matarese, A., and Santulli, G. (2019). Cardiosomal microRNAs are essential in post-infarction myofibroblast phenoconversion. Int. J. Mol. Sci. *21*, 201. https://doi.org/10.3390/ijms21010201.

82. Matarese, A., Gambardella, J., Sardu, C., and Santulli, G. (2020). miR-98 regulates TMPRSS2 expression in human endothelial cells: key implications for COVID-19. Biomedicines *8*, 462. https://doi.org/10.3390/biomedicines8110462.

83. Wang, X., Morelli, M.B., Matarese, A., Sardu, C., and Santulli, G. (2020). Cardiomyocyte-derived exosomal microRNA-92a mediates post-ischemic myofibroblast activation both in vitro and ex vivo. ESC Heart Fail. *7*, 284–288. https://doi.org/10.1002/ehf2.12584.

84. Kansakar, U., Gambardella, J., Varzideh, F., Avvisato, R., Jankauskas, S.S., Mone, P., Matarese, A., and Santulli, G. (2022). miR-142 targets TIM-1 in human endothelial cells: potential implications for stroke, COVID-19, Zika, Ebola, Dengue, and other viral infections. Int. J. Mol. Sci. *23*, 10242. https://doi.org/10.3390/ijms231810242.

85. Gambardella, J., and Fiordelisi, A., Spigno L., Boldrini L., Lungonelli G., Di Vaia E., Santulli G., Sorriento D., Cerasuolo F.A., Trimarco V., Iaccarino G. (2021). Effects of chronic supplementation of L-Arginine on physical fitness in water polo players. Oxid Med Cell Longev. *2021*, 6684568. https://doi.org/10.1155/2021/6684568.

86. Lombardi, A., Gambardella, J., Du, X.L., Sorriento, D., Mauro, M., Iaccarino, G., Trimarco, B., and Santulli, G. (2017). Sirolimus induces depletion of intracellular calcium stores and mitochondrial dysfunction in pancreatic beta cells. Sci. Rep. *7*, 15823. https://doi.org/10.1038/s41598-017-15283-y.

87. Lombardi, A., Trimarco, B., Iaccarino, G., and Santulli, G. (2017). Impaired mitochondrial calcium uptake caused by tacrolimus underlies beta-cell failure. Cell Commun. Signal. *15*, 47. https://doi.org/10.1186/s12964-017-0203-0.

88. Santulli, G., Wronska, A., Uryu, K., Diacovo, T.G., Gao, M., Marx, S.O., Kitajewski, J., Chilton, J.M., Akat, K.M., Tuschl, T., et al. (2014). A selective microRNA-based strategy inhibits restenosis while preserving endothelial function. J. Clin. Invest. *124*, 4102–4114. https://doi.org/10.1172/JCI76069.

89. Iaccarino, G., Ciccarelli, M., Sorriento, D., Cipolletta, E., Cerullo, V., Iovino, G.L., Paudice, A., Elia, A., Santulli, G., Campanile, A., et al. (2004). AKT participates in endothelial dysfunction in hypertension. Circulation *109*, 2587–2593. https://doi.org/10.1161/01.CIR.0000129768.35536.FA.

90. Santulli, G., Xie, W., Reiken, S.R., and Marks, A.R. (2015). Mitochondrial calcium overload is a key determinant in heart failure. Proc. Natl. Acad. Sci. USA. *112*, 11389–11394. https://doi.org/10.1073/pnas.1513047112.

91. Gambardella, J., Coppola, A., Izzo, R., Fiorentino, G., Trimarco, B., and Santulli, G. (2021). Role of endothelial miR-24 in COVID-19 cerebrovascular events. Crit. Care *25*, 306. https://doi.org/10.1186/s13054-021-03731-1.

STAR★METHODS

KEY RESOURCES TABLE

REAGENT or RESOURCE	SOURCE	IDENTIFIER
Antibodies		
Mouse monoclonal anti-PHD2	Santacruz Biotechnology	Cat# SC-271835; RRID:AB_10709895
Mouse monoclonal anti-GAPDH	Santacruz Biotechnology	Cat# SC-365062; RRID:AB_10847862
Mouse monoclonal anti-HIF1ALPHA	Novusbio	Cat# NB100-105; RRID:AB_10001154
Rabbit monoclonal anti-HEXOKINASE	Cell Signaling Technology	Cat# 2867S; RRID:AB_2232946
Mouse monoclonal anti-PDK1	Santacruz Biotechnology	Cat# SC-293160;
Rabbit monoclonal anti-GLUT1	abcam	Cat# AB115730; RRID:AB_10903230
Mouse monoclonal anti-Gα i-1	Santacruz Biotechnology	Cat# SC-13533; RRID:AB_2111358
Mouse monoclonal anti- a-ACTIN	Santacruz Biotechnology	Cat# SC-130616; RRID:AB_1561784
Mouse monoclonal anti-LDH-1	Santacruz Biotechnology	Cat# SC-133123; RRID:AB_2134964
Rabbit polyclonal anti-GLUT-4	abcam	Cat# AB-37445; RRID:AB_732612
Biological samples		
Human Blood	This paper Federico II University Hospital, Fabry clinic	N/A
Skin Biopsy	This paper, Federico II University Hospital, Fabry clinic	N/A
Chemicals, peptides, and recombinant proteins		
Dulbecco's Modified Eagle Medium (DMEM), High Glucose	Microgem	AL007-500ML
Lipofectamine™ 2000 Transfection Reagent	Invitrogen™	11668-019
Critical commercial assays		
PowerTrack™ SYBR Green Master Mix	Applied Biosystems™ Thermo Fisher	A46109
SuperScript™ VILO™ Master Mix	Invitrogen	11755-050
*mir*Vana™ miRNA Isolation Kit	Invitrogen	AM1560
Lactate Assay Kit	Sigma-Aldrich	MAK064
Deposited data		
Mass spectrometry raw data for lipidomic analysis	This paper	Zenodo https://doi.org/10.5281/zenodo.7347754
Experimental models: Cell lines		
Patients derived Fibroblasts (Isolated from skin biopsy)	This paper	N/A
Experimental models: Organisms/strains		
Mouse: Fabry mice (hR301Q α-Gal A Tg/KO C57BL/6N backcrossed)	This paper	N/A
Mouse: Control mice (negative hR301Q α-Gal A Tg/WT C57BL/6N backcrossed)	This paper	N/A
Oligonucleotides		
Primers for Genotyping: GLA-KO, Human-GLA Tg See Table S1	This paper	N/A
Primers for 18s See Table S2	This paper	N/A
Primers for FASN See Table S2	This paper	N/A

(*Continued on next page*)

Continued

REAGENT or RESOURCE	SOURCE	IDENTIFIER
HIF-1 siRNA	Santacruz Biotechnology	SC-35561
ANTAGOMIR17	Ambion	4464084 ID:MH12412
Software and algorithms		
ImageJ	NIH; Schneider et al., 2012[64]	https://imagej.nih.gov/ij/
GraphPad	Prism (Dotmatics)	https://www.graphpad.com/scientific-software/prism/

RESOURCE AVAILABILITY

Lead contact

Further information and requests for resources and reagents should be directed to and will be fulfilled by the lead contact, Guido Iaccarino (MD, PhD, Federico II University, Napoli, Italy: guiaccar@unina.it).

Material availability

The materials underlying this article will be shared upon reasonable request to the lead contact, Guido Iaccarino.

Data and code availability

Lipidomic data generated by this study are publicly available at the Zenodo database with the identifier: 7347754 (key words: Lipidomics, metabolomics, Fabry Disease, FT-ICR-MS, UHPLC-TIMS-qTOF). This study did not generate any code. Additional information required to reanalyze the data reported in this paper is available from the lead contact upon request.

EXPERIMENTAL MODEL AND SUBJECT DETAILS

Human study population

The human study was approved by the Institutional ethical committee of Federico II Hospital (Protocol n. 181/19). Written informed consent was received prior to participation. Patients of both sexes with confirmed FD diagnoses were recruited in the FD Clinic of AOU Federico II; healthy controls were recruited in the Sports Medicine Clinic of AOU Federico II. FD patients met the following inclusion criteria: Adult $\geq$18 years of age, confirmed diagnosis of classic FD, subscription of informed consent. We excluded patients with late-onset or non-classical variants of FD and patients in treatment with beta-blockers. We cumulatively considered patients and matched controls of both sexes. Table 1 summarizes the main clinical characteristics of our study populations. Controls were age and sex-matched with a ratio of 2:1. The diagnostic algorithm for FD is based on the measurement of α-Gal A activity, which is recommended in males and optional in females, and on the genetic confirmatory testing, which is mandatory in both genders.[65] In our population, 40% of FD patients had a nonsense mutation in α-Gal A gene, introducing a premature stop codon that produces a protein truncation at aminoacidic residue 301 (p. Arg301*). The other 60% of patients is characterized by different types of missense mutations. The complete panel of α-Gal A gene mutations detected in our FD population is reported in Table 2.

Animals

Animal husbandry and all experiments were conducted under Institutional Animal Care and Use Committee approved protocols by Federico II University of Naples (Protocol n. 294/2020-PR). Homozygous Tg/KO mice that express a mutant form of human α-Gal A (R301Q) on a GLA KO mixed background of C57BL/6N and B129Sve (hR301Q α-Gal A Tg/KO), were backcrossed into a C57BL/6N background. After five generations, we obtained homozygous for α-Gal A KO and R301Q-Tg insertion and syngeneic negative littermates as control mice.

For genotyping, we performed PCR on genomic DNA from the mouse tail using Primer 1 and 2 to amplify the wild-type allele generating a 400-bp fragment. To detect the knock-out construct, Primer 1 and Primer 3 were used to amplify a 600-bp fragment (Figure S3A). The PCR protocol consisted of 30 cycles of denaturation at 94°C for 30 seconds, annealing at 59°C for 30 seconds, and elongation at 72°C for 30 seconds. The

presence of Tg-R301Q was confirmed by using primers T1 and T2, generating a 231-bp fragment (Figure S4A). Briefly, the PCR protocol consisted of 30 cycles of denaturation at 94°C for 30 seconds, annealing at 60°C for 30 seconds, and elongation at 72°C for 30 seconds. Homozygosity of transgene R301Q was discriminated by performing quantitative Real-time PCR for Tg-R301Q, by using 18s as a housekeeping reference gene. DNA isolated from original FD mice (homozygous for Tg-R301Q), from II generation mice (heterozygous for Tg-R301Q), and WT mice (negative for Tg-R301Q) was used as a reference sample to assess the relative expression amount of tg during screening procedure (Figure S4B). All primer sequences used to genotype are reported in Table S1.

For all experimental procedures, we used male and female 6 monthsold Tg/KO mice (FD mice) and age-matched negative littermates (WT-wildtype for GLA and negative for R301Q-Tg) as the control group. In preliminary results, no effect of sex was observed in muscle phenotype between male and female mice.

Cell culture

Primary fibroblasts were obtained from skin biopsies. One FD patient (male patient) and a healthy first-degree relative (a donator from the same family but not inheriting the GLA mutation). The skin biopsies were cut (1 mm × 3 mm) into small pieces using a scalpel blade and cultivated on cell culture dishes coated with 0,1% of gelatin in fibroblast medium, consisting of DMEM supplemented with 20% FBS, 2 mM L-glutamine and 1% penicillin and streptomycin (all from Invitrogen), as we previously described.[66] After 3 passages, cells were collected and processed for further analyses.

METHOD DETAILS

Determination of exercise tolerance in patients

Patients were subjected to an exercise tolerance test using the Bruce protocol on a cycle ergometer.[67] The test was stopped at 85% of theoretical heart rate or exhaustion. METs, double products, and duration were analyzed to determine the tolerance to exercise. Circulating lactate levels were measured at rest and peak of effort through the StatStrip Lactate System (Nova Biomedical), to associate lactate accumulation with exercise tolerance.[68]

Plasma metabolome and lipidome extraction

Peripheral blood was collected after overnight fasting from FD patients and controls, anticoagulated with EDTA, and centrifuged at 2000 rpm for 10 min to obtain plasma. Metabolites and lipids were extracted from plasma following the Matyash et al. protocol[69] with slight modifications. Briefly, 20 μL of plasma were thawed on ice and added to 225 μL of ice-cold MeOH and vortexed for 10 s. Subsequently, 750 μL of ice-cold MTBE were transferred to the tube and the solution was shacked in a thermomixer (Eppendorf) for 10 min, 300 rpmat 4°C. Then, 188 μL of H_2O were added and samples were vortexed for 20 s and centrifuged at 14680 rpm, for 10minat 4°C to induce phase separation. The upper (lipids) and lower (polar metabolites) layers were collected and evaporated using a SpeedVac (Savant, ThermoFisher Scientific, Waltham, MA). A quality control (QC) sample was prepared by pooling the same aliquot (3 μL) from each sample. Unless otherwise described, all solvents and additives were LC-MS grade and purchased by Merck (Darmstadt, Germany).

FIA-FT-ICR metabolome analysis

FIA-FT-ICR analyses were performed in flow injection analysis using an Ultimate 3000 RSLC coupled to SolariX XR 7T (Bruker Daltonics, Bremen, Germany). The flow rate was set to 10 μL/min and a step wash of 0.3 min was performed at 300 μL/min during the wash phase. The instrument was tuned with a standard solution of sodium trifluoracetate (NaTFA). Mass spectra were recorded in a broadband mode in the range of 90–1000 m/z, with an ion accumulation of 70 ms, 32 scans were acquired using 2 million data points (2 M), with a resolution of 150.000 at m/z 400. Drying gas (N_2) was set at 4 L/min, with a drying temperature of 200°C. Funnel RF amplitude was set to 100.0 Vpp and RF amplitude TOF was 350.0 Vpp, TOF was set to 0.6 ms, and RF frequency transfer optic 4 MHz. Both positive and negative ESI ionization was employed in separate runs. The instrument was controlled by Bruker FTMS Control (Bruker Daltonics).

RP-UHPLC-TIMS-MS lipidome analysis

UHPLC-TIMS analyses were performed on a Thermo Ultimate RS 3000 coupled online to a TimsTOF Pro quadrupole Time of flight (Q-TOF) (Bruker) equipped with an Apollo II electrospray ionization (ESI) probe.

The separation was performed with an Acquity UPLC CSH C18 column (100 × 2.1 mm; 1.7 μm) protected with a VanGuard CSH precolumn (5.0 × 2.1 mm; 1.7 μm, 130 Å) (Waters, Milford, MA). The column temperature was set at 55°C, a flow rate of 0.4 mL/min was used, mobile phase consisted of (A): ACN/H_2O with 10 mM $HCOONH_4$ and 0.1% HCOOH 60:40 (v/v) and (B): IPA/ACN with 10 mM $HCOONH_4$ and 0.1% HCOOH 90:10 (v/v). The following gradient has been used: 0 min, 40% B; 2 min, 43% B; 2.10 min, 50% B; 12 min, 54% B; 12.10 min, 70% B; 17 min, 99% B; 17.10 min, 99% B; 17.2, 40% B and then 2.8 min for column re-equilibration. The analyses were performed in data-dependent parallel accumulation serial fragmentation (DDA-PASEF) with both positive and negative ionization, in separate runs. The injection volume was set at 3 μL for the positive mode and 5 μL for the negative mode. Source parameters: Nebulizer gas (N_2) pressure: 4.0 Bar, Dry gas (N_2): 10 L/min, Dry temperature: 250°C. Mass spectra were recorded in the range m/z 100–1500, with an accumulation and ramp time of 100 ms each. The ion mobility was scanned from 0.55 to 1.70 Vs/cm^2. Precursors for data-dependent acquisition were isolated within ±2 m/z and fragmented with a fixed ion collision energy, 30 eV in positive mode and 40 eV in negative mode. The total acquisition cycle was 0.32 s and comprised one full TIMS-MS scan and two PASEF MS/MS scans. Exclusion time was set to 0.1 min, and Ion charge control (ICC) was set to 7.5 Mio. The instrument was calibrated for both mass and mobility using the ESI-L Low Concentration Tuning Mix with the following composition: [m/z, $1/K_0$: (322.0481, 0.7318 Vs cm^{-2}), (622.0290, 0.9848 Vs cm^{-2}), (922.0098, 1.1895 Vs cm^{-2}), (1221,9906, 1.3820 Vs cm^{-2})] in positive mode and [m/z, $1/K_0$: (301.99814, 0.6678 Vs cm^{-2}), (601.97897, 0.8781 Vs cm^{-2}), (1033.98811, 1.2525 Vs cm^{-2}), (1333.96894, 1.4015 Vs cm^{-2})] in negative mode.

HRMS data analysis and processing

UHPLC-TIMS and FIA-FT-ICR lipidomics and metabolomics data alignment, filtering, and annotation were performed with MetaboScape 2021 (Bruker) as follows: for lipidomics, the algorithm T-Rex 4D was used, which automatically extracts buckets from raw files. For lipidomics, at the beginning of each LC-MS run, a mixture (1:1 v/v) of 10 mM sodium formate calibrant solution and ESI-L Low Concentration Tuning Mix was injected to recalibrate, respectively, both the mass and mobility data. Feature detection was set to 500 and 250 counts for positive and negative modes. The minimum number of data points in the 4D TIMS space was set to 100, and recursive feature extraction was used (75 points). Lipid annotation was performed first with a Rule-based annotation and, subsequently, using the LipidBlast spectral library of MS DIAL (http://prime.psc.riken.jp/compms/msdial/main.html) with the following parameters: tolerance: narrow 2 ppm, wide 10 ppm; mSigma: narrow 30, wide 250, MS/MS score: narrow 800, wide 150. CCS%: narrow 2, wide 5. The spectra were processed in positive mode using $[M+H]^+$, $[M+Na]^+$, $[M+K]^+$, $[M+H-H_2O]^+$ and $[M+NH_4]^+$ ions in positive mode, while $[M–H]^-$, $[M+Cl]^-$, $[M+HCOO]^-$ and $[M-H_2O]^-$ in negative mode. CCS values were further compared with those predicted by LipidCSS tool (http://www.metabolomics-shanghai.org/LipidCCS/), and the assignment of the molecular formula was performed for the detected features using Smart Formula™ (SF). For the assessment of repeatability and instrument stability over time, a QC strategy was applied[70] using pooled samples at different dilution levels (1:1, 1:10) and inserted during the batch regularly.

Metabolomics data analysis was also performed with MetaboScape 2021. The first step is the creation of a matrix (bucket table) using the T-ReX 2D algorithm. The T-Rex 2D algorithm for feature extraction from FT-ICR single spectra extracts m/z/intensity pairs (peaks) from acquired raw data and subjects them to deisotoping to create features consisting of isotope patterns. Subsequently, spectra alignment, filtering, and normalization were performed. The spectra were processed in positive mode using H^+ as the primary ion, Na^+ and K^+ as a potential adduct, while in negative mode H^- was set as the primary ion and Cl^- as a potential adduct. For metabolite annotation, assignment of the molecular formula was performed for the detected features using Smart Formula™ (SF), and isotopic fine structure (ISF). The bucket table was annotated with a list of metabolites and lipids obtained respectively from the HMDB (https://hmdb.ca/) and LIPIDMAPS database (www.lipidmaps.org). Annotation was performed with 0.2 ppm (narrow) or 1 ppm (wide) mass tolerance and a mSigma value below 200, molecular formulas were manually inspected taking into account the most probable adduct form.

Univariate and multivariate statistical analyses were conducted with normalized and scaled HRMS data using MetaboAnalyst (v. 5.0, http://www.metaboanalyst.ca/), data from both ionization polarities were treated simultaneously. One-way ANOVA with Tukey *post hoc* test was performed for inter-group comparisons with false discovery rate (FDR) correction. Explorative analysis was performed by principal component analysis (PCA) while partial least square discriminant analysis (PLS-DA). PLS-DA was used as a classification

model to graphically describe the classes separation and to extract relevant metabolites defined as the ones showing variable importance in projection (VIP) scores higher than 1. The validity and robustness of the PLS-DA model were evaluated using the coefficient R^2 (model-fit) and the coefficient Q^2 (predictive ability), respectively, using the 5-fold internal cross-validation method. Heat maps and whisker boxplots were used to highlight the most significant metabolites.

Detection of miR-17 levels

miR-17 levels were determined in plasma from FD patients compared to healthy controls, and plasma from FD mice compared to Wild-type. Peripheral blood was collected from patients and mice in EDTA-tubes and plasma was obtained by centrifugation as we previously reported.[27] We extracted microRNAs using the miRVana miRNA isolation kit (ThermoFisher Scientific) according to the manufacturer's protocol; the quality of miRNA was determined using Agilent Small RNA Kit.[27,71]

Spontaneous activity recording

Voluntary wheel-running activity was used as a surrogate measure of exercise capacity and tolerance.[72] Specifically, mice were allowed to run freely on the plastic wheel placed inside a standard mouse cage. After 1 day of adaption, the number of rotations was automatically recorded by the cage wheel running system provided by Columbus Instruments (Columbus, OH). The software acquired data on the total number of wheel revolutions performed every hour for a 16-hour overnight period.[72] Following data collection, mice were returned to cages without a running wheel for at least 3 days before *ex vivo* experiments.

Weight test

The weight test was performed as previously described.[73] Briefly, the exercise was articulated in seven stages in which the mice needed to hold growing weights (20, 33, 46, 59, 72, 85, and 98 g). Ahold of three seconds was the criterion; if the mouse was able to hold the weight for 3 seconds, then it went to the next step, if not after three chances the exercise stopped. The score was then assigned considering the stage achieved and the time of holding of the last step (3 points per completed steps, + holding seconds of the last step). Following data collection, mice were returned to cages for at least 3 days before *ex vivo* experiments.

Glucose tolerance test

After 6 hours of fasting, FD and WT mice were subjected to a glucose tolerance test (GTT) through intraperitoneal glucose injection (2 g/kg i.p).[74–76] Blood glucose levels were measured by tail bleeding (Glucose Analyzer II; Beckman Coulter, Brea, CA, USA) at the indicated time points.

Muscle dissection and protein extraction

At 6 months FD and WT mice were euthanized and the femoral quadriceps muscle was isolated and immediately frozen in liquid nitrogen.[72,77] 20 mg of frozen tissue were homogenized with a Polytron (Brinkman Instruments, Riverview, FL, USA) in ice-cold RIPA/SDS buffer (50 × 10^{-3} mol/L Tris-HCl (pH 7.5), 150 × 10^{-3} mol/L NaCl, 0.01 g/L NP-40, 0.0025 g/L deoxycholate, 2 × 10−3 mol/L Na_3VO_4, 0.2 g/L sodium, 2 × 10−3 mol/L EDTA, 2 × 10−3 mol/L PMSF), for whole protein extraction. To isolate plasma membrane, samples were homogenized in Tris (pH 7.5 25 × 10^{-3} mol/L)/EDTA (5 × 10^{-3} mol/L)/EGTA (5 × 10^{-3} mol/L) buffer, and a protocol of differential centrifugation was used to obtain cell membrane pellet as previously described.[78] All lysis buffers also contained fresh phosphatase inhibitors (Sigma-Aldrich, Saint Lois, MI, USA). Protein concentration was determined using the Bradford Protein Assay (Bio-Rad, Hercules, CA, USA).

Immunofluorescence on muscle tissue

For the determination of muscle fibers composition, immunofluorescence analysis[79] was performed on cryostat sections from femoral muscle. Briefly, cryostat sections were fixed in cold methanol, blocked in BSA 1%, and incubated with monoclonal antibodies specific for the different myosin isoforms (MyHC1, MyHC2a, MyHC2b) (Biolegends). This strategy allowed us to discriminate the amount of oxidative, glycolytic, and intermediate fibers. Immunofluorescence analysis was also performed on cryostat sections to determine the number of muscle fibers positive for glucose transporters Glut1/4 (Abcam) and CD36 (R&D).

Intramuscolar lactate determination

Muscle tissue isolated from FD and WT mice was homogenized in RIPA buffer and centrifuged to eliminate debris. Lactate concentration was determined by using a colorimetric assay kit provided by Merck (Darmstadt, Germany). Briefly, the muscle lysate was used as a substrate for an enzymatic reaction that results in a colorimetric (450 nm) product, proportional to the lactate present in the sample. For reagent concentration and timing we followed the manufacturer's instructions. Levels of lactate in each sample were normalized by protein concentration.

HIF-1 siRNA and AntagomiR-17 transfection

The day before transfection the cells were counted and seeded in 6-well plates (2×10^5 cells per well). For HIF-1 silencing we used 60 nmol of HIF-1 siRNA duplex provided by Santacruz Biotechnology, for 48 hours, while control siRNA respectively (Vehicle) was used to contextually transfect control cells.[75,80] For AntagomiR-17 transfection, 30 nM of control antagomiR (CTRL) or human AntagomiR-17 purchased from Ambion were used. In both cases, the transfection was conducted using lipofectamine for RNAiMAX (Invitrogen), and OptiMEM medium following the manufacturer's instructions.[81–84] 48 hours after transfection, FD cells were collected and processed for further biochemical assays.

In vitro evaluation of glucose consumption and lactate production

Control and FD fibroblasts were counted and seeded at a density of 2×10^5 cells per well in the 6-well plates. The day after, the medium was changed with fresh culture medium and the cells incubated for 48 hours. Then, cell medium was collected and after centrifugation to remove cells in suspension (1000 g × 5 min at 4°C), the cell supernatant was analyzed by AutomaticQC Cartridge (RapidPoint 500e, Siemens) analyzer to determine glucose and lactate concentration. Both parameters were normalized for the cell number determined for each well by cell counter after trypsinization. The culture medium incubated for the same time without cells was used as control to determine the initial amount of glucose and lactate and to obtain, by subtraction, the rate of glucose consumption and lactate release by,respectively, control and FD fibroblasts.

Assessment of extracellular acidification rate (ECAR)

ECAR is an indicator of glycolysis, since when lactate derived from glycolysis is released from cells also protons are released. Control and FD fibroblasts were seeded on 96-well plates at a density of 2×10^4 cells per well. After 24h of incubation, ECAR was measured for glycolytic metabolism assessment by using the Seahorse XFe96 extracellular flux analyzer (Seahorse Bioscience, Agilent Technologies, Santa Clara, CA, USA). Through a sensor cartridge, pH modifications are recorded in real-time in live cells as previously described.[85–87]

Western blot analysis

An equal amount of protein from each sample (30 μg) was used for immunoblot analysis.[78,79,88] Briefly, whole extract or membrane proteins were separated by 4–12% SDS/PAGE gel and transferred to an Immobilon-P nitrocellulose filter (*Millipore*); the membranes were blocked in Tris-buffered saline containing 0.002 g/l Tween 20 (TBST) and 0.05 g/l non-fat dry milk. After blocking, the membranes were washed three times with TBST and then incubated overnight at 4°C in 5% BSA TBST with primary antibodies specific for HK, PDK1, LDH1, HIF-1α (*Cell Signaling*), PHD2 (*SantaCruz Biotechnologies*) on total extracts, or Glut 4-1 (*abcam*) on membrane extract. Actin, GAPDH and $G\alpha_i$ (*SantaCruz Biotechnologies*) levels were used as loading control for total or membrane extract respectively. Secondary peroxidase-conjugated antibodies (*ImmunoReagents*) were used to visualize the antigen-antibody complexes on a nitrocellulose filter by chemiluminescence. A standard chemiluminescence reaction kit (Pierce) was used for autoradiography on film.

Real-time PCR

Gene expression levels were determined by real-time reverse transcription-polymerase chain reaction (RT-qPCR) as previously described and validated.[77,89–91] Briefly, RNA extraction was performed from 50 mg of muscle tissue by TRIzol Reagent (Invitrogen, Carsbad, CA, USA). The amount of isolated RNA was dissolved in 50 μL of RNAse-free water and the concentration was determined by a micro-Volume spectrophotometer (MaestroGen, Carson City, NV). 2 μg of RNA for each sample was retro-transcripted by a One-Step RT-PCR kit (Vilo, Invitrogen). The RT-qPCR was then performed with a StepOne System-Applied Byosistem

(ThermoFisher Scientific) using SyberGreen as identification method. In each amplification tube, a total volume reaction of 20 μL was composed by: 20 ng of synthetized cDNA (in a volume of 2 μL), 10 μL of BrightGreen 2X qPCR MasterMix-ROX (Applied Biological Material - abm, Richmond, BC, Canada), and 2 μL of forward and reverse 500 nM stock primers. Each tube was prepared in triplicates, and the RT-qPCR assay for 18S and FASN were performed with the primers listed in Table S2. Each RT-qPCR cycle consisted of heating at 95°C for 15 s, 60°C for 30 s for annealing, and 72°C for 1 min for the extension. At the end of the reaction, melting curve analysis was performed to evaluate the specificity of the amplification reaction for each primer pair. The levels of 18S mRNA were used for normalization. The gene expression levels for each target gene were determined using the comparative Ct method normalized for 18S.[74]

QUANTIFICATION AND STATISTICAL ANALYSIS

All experiments were performed at least in triplicate by blinded investigators. Shapiro-Wilk test was applied to verify the normal distribution of values; unpaired t-test or ANOVA followed by Bonferroni or Tukey *post hoc* testing were performed as appropriate, where applicable. A significance level of $p < 0.05$ was assumed for all statistical evaluations. Statistics were computed with GraphPad Prism (v. 8.4.0) software (San Diego, CA).